

Local charge compensation from colour preconfinement as a key to the dynamics of hadronization

Kosuke Odagiri

Institute of Physics, Academia Sinica, Nankang, Taipei, Taiwan 11529, The Republic of China

ABSTRACT: If, as is commonly accepted, the colour-singlet, ‘preconfined’, perturbative clusters are the primary units of hadronization, then the electric charge is necessarily compensated locally at the scale of the typical cluster mass. As a result, the minijet electric charge is suppressed at scales that are greater than the cluster mass. We hence argue, and demonstrate by means of Monte Carlo simulations using HERWIG, that the scale at which charge compensation is violated is close to the mass of the clusters involved in hadronization, and its measurement would provide a clue to resolving the nature of the dynamics. We repeat the calculation using PYTHIA and find that the numbers produced by the two generators are similar. The cluster mass distribution is sensitive to soft emission that is considered unresolved in the parton shower phase. We discuss how the description of the splitting of large clusters in terms of unresolved emission modifies the algorithm of HERWIG, and relate the findings to the yet unknown underlying nonperturbative mechanism. In particular, we propose a form of α_S that follows from a power-enhanced beta function, and discuss how this α_S that governs unresolved emission may be related to power corrections. Our findings are in agreement with experimental data.

KEYWORDS: qcd.jet.

Contents

1. Introduction	1
2. Colour preconfinement and charge compensation	2
3. Charge compensation observables	3
4. Result of simulations	5
5. Interpretation in terms of cluster dynamics	16
6. Interpretation of low energy α_S	24
7. Conclusions	33

1. Introduction

Hadronization is one of the most poorly understood aspects of QCD. Our knowledge is currently limited to models [1, 2] and estimations of the power-suppressed corrections [3] to observables that have sensitivity to soft physics.

Of the little that is known about the dynamics of hadronization, colour preconfinement [4, 5], which is a general property of perturbative QCD, is often regarded as a plausible starting point.

Colour preconfinement is a theorem, which follows from perturbative QCD, that states that in the course of the evolution between the hard scale Q_{hard} and the cut-off scale Q_0 that results in the formation of a perturbative parton shower, the quarks and gluons become organized in colour-singlet ‘clusters’, whose mass is of order Q_0 and is independent of Q_{hard} in the limit of large Q_{hard} .

It has been proposed [4] that the clusters so produced participate independently in hadronization. If so, and provided that the physical cut-off scale to the parton shower is found to be small compared with Q_{hard} , the nonperturbative contribution to jets should not dramatically disturb the properties of the perturbative parton shower.

Models of hadronization based on colour preconfinement, notably the Monte Carlo event generators HERWIG [1] and PYTHIA [2], have been found to agree, to within creditable accuracy, with experimental data. When carrying out this comparison, since the dynamics of hadronization is little understood, it is necessary to tune some parameters that are related to hadronization.

One of the key parameters is the cut-off scale Q_0 , above which it is appropriate to apply the perturbative parton shower evolution and below which nonperturbative dynamics dominates.

By means of experimental tunes it has been discovered that the cut-off scale is quite low, $\mathcal{O}(1 \text{ GeV})$. Thus the typical cluster mass is also small.

Despite the success of the models of hadronization based on preconfinement, the existence of these preconfined clusters hitherto lacks direct experimental evidence¹. In view of this, we turn our attention to the phenomenon of local charge compensation [7]. We demonstrate that colour preconfinement naturally leads to local charge compensation. We advocate the measurement of minijet charge rather than distribution in rapidity space which has been traditionally considered. This change of observable allows us to relate the scale of charge compensation to the scale of colour preconfinement.

In HERWIG, the perturbative clusters that remain large at the end of the parton shower phase are split according to a parametrization. We point out that because the mass distribution of the clusters is sensitive to soft emission that is considered unresolved in the parton shower phase, this cluster-splitting dynamics may be rephrased in terms of unresolved emission governed by a modified low energy running strong coupling. By comparing the result with the default cluster mass distribution of HERWIG, we can estimate the energy scale involved in the cluster-splitting phase, or the shape of the modified α_S , and derive a possible phenomenological distinction.

The cluster splitting energy scale thus established may be interpreted loosely as the scale of ‘emission before confinement’. We discuss one explicit interpretation where enhanced $g \rightarrow q\bar{q}$ splitting modifies the running of α_S . The resulting form of low-energy α_S agrees with our findings with physically acceptable parameter values. We then discuss how this α_S relates to the part of the power corrections that is due to soft gluon emission. As the α_S has complex poles, there is ambiguity associated with its analytization.

This paper is organized as follows. We first introduce the concept of colour preconfinement and the resulting local compensation of charge. We proceed to define the relevant observables. We carry out simulations using the HERWIG Monte Carlo event generator and compare the numbers against those of PYTHIA. We discuss the cluster-splitting procedure in HERWIG that affects this observable, and consider possible physics interpretations and consequences. Conclusions are stated at the end.

2. Colour preconfinement and charge compensation

In the original proposal of Amati and Veneziano [4], units composed of perturbatively emitted quarks and gluons become colour-singlet clusters. Obviously the ‘ends’ of these clusters are defined by quarks. However, as the emission of quarks in a parton shower is a relatively rare event, the resultant clusters can be quite large even though the mass is still determined by Q_0 in the limit of large Q_{hard} . In the Lund string model of PYTHIA, these quark-gluon systems are regarded as ‘kinked strings’ that subsequently decay into hadrons.

¹However, we note that the minijet structure of jets has been studied in the context of cluster hadronization in ref. [6]

An alternative, and more economical, approach adopted in the cluster hadronization model [8] of HERWIG is to introduce forced, ‘nonperturbative’, splitting of gluons at the end of the parton shower, such that all clusters are quark-antiquark colour-singlet dipole systems. However, even in this case, there often remain in the end some clusters that are considered too large to be nonperturbative objects. These clusters are then split by a power distribution in terms of the masses of the decay products. We shall discuss this in more detail in secs. 4 and 5. The small clusters at the end decay isotropically into hadrons according to the phase space weight.

We may therefore say that the primary units of hadronization are, in the former picture, perturbative colour-singlet systems, whereas in the latter, all colour connected two-parton systems, or in other words, dipoles.

In any case, if the physical cut-off scale is at $Q_{0(\text{physical})}$, then for all artificial cut-off scales Q_0 greater than $Q_{0(\text{physical})}$, emitted partons are organized into clusters with mass of order Q_0 . Therefore if we take an observable that is insensitive to physics below Q_0 , we would be measuring the properties of clusters with mass of order Q_0 .

The electric charge of a cluster is always 0 or ± 1 because a cluster is in effect a quark-antiquark system. Following our reasoning above, the charge is 0 or ± 1 at all scales above $Q_{0(\text{physical})}$, such that if a cluster at a certain scale is composed of a number of smaller clusters at a smaller scale, the electric charges of these smaller clusters must mutually cancel.

Hence electric charge is ‘locally’ compensated if colour is preconfined, rather than increasing in proportion to the square root of the number of charged tracks belonging to the cluster as would be expected if the charges were uncorrelated. It is worth noting that the converse is not necessarily true. In particular, in PYTHIA, although the strings may be quite large, their decay proceeds by the creation of quark-antiquark pairs, such that the scale at which charge is compensated is in general small compared to the mass of the strings.

At scales lower than $Q_{0(\text{physical})}$, on the other hand, if nonperturbative effects are dominant, there is no reason to expect that charge is locally compensated. This is illustrated in fig. 1.

3. Charge compensation observables

In practice, it is not possible to define an exclusive observable that is absolutely independent of physics below a certain arbitrary scale. However, we would physically expect that a minijet charge, if appropriately defined, can minimize the contamination.

The sensitivity to physics below the scale defined by the minijet resolution variable depends on the algorithm that is used to combine tracks or objects consisting of tracks. We expect that k_T based algorithms [9, 10] exhibit the most desirable properties since the resolution variable k_T defined between two objects is, in principle, the energy scale that is required for a splitting that creates the two objects. In view of this, let us as our default procedure adopt the Cambridge [10] algorithm. This algorithm adopts as the test variable

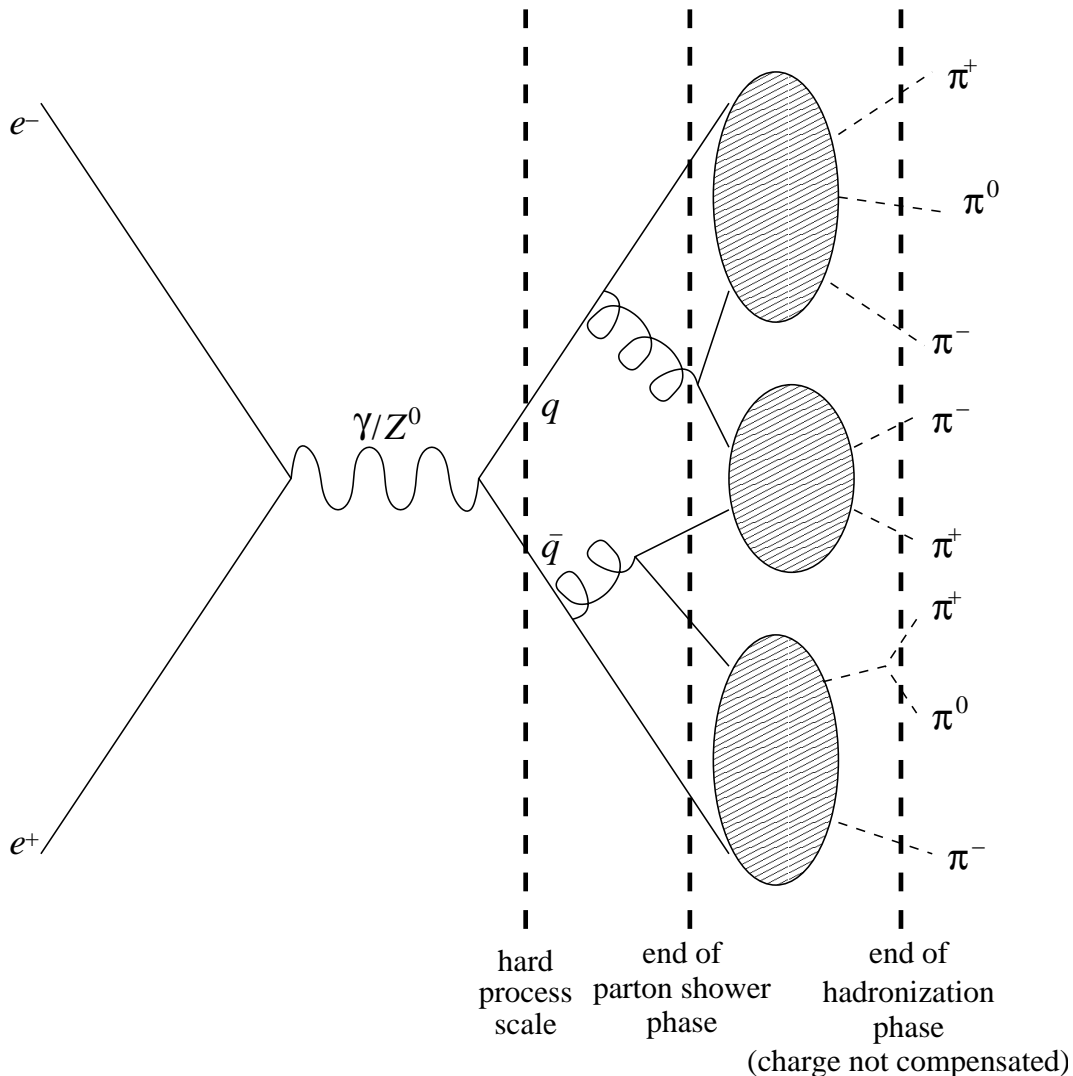


Figure 1: An illustration of the violation of local charge compensation during hadronization in the colour preconfinement picture (HERWIG). Neighbouring charges do not necessarily cancel.

between objects (ij) a variable that is essentially k_T^2 :

$$y_{ij} \propto \min(E_i, E_j)^2 v_{ij}. \quad (3.1)$$

The normalization factor is taken to be $1/E_{\text{vis}}^2$ where E_{vis} is the total visible energy. The quantity v_{ij} , which also serves as the ordering variable, is defined by:

$$v_{ij} = 2(1 - \cos \theta_{ij}). \quad (3.2)$$

The jet construction algorithm is iterative and the pair (ij) with the smallest value of v_{ij} that satisfies $y_{ij} < y_{\text{cut}}$ is combined. In addition, for a pair which does not satisfy $y_{ij} < y_{\text{cut}}$ but have smaller values of v_{ij} , the object with lower energy is ‘frozen’ by regarding this object as a jet. This last point marks the distinction between the Cambridge algorithm and the ‘angular-ordered Durham’ algorithm [10].

We now define the minijet charge as

$$Q_{\text{minijet}}(y_{\text{cut}}) = \sum Q_{\text{track}}. \quad (3.3)$$

The summation is over the tracks that belong to the minijet under consideration. It is also instructive to define a charge that is weighted by powers of the track three-momenta, as:

$$Q_{\text{minijet}}(y_{\text{cut}}, \kappa) = \frac{\sum Q_{\text{track}} (P_{\text{track}} \cdot P_{\text{minijet}})^\kappa}{\sum (P_{\text{track}} \cdot P_{\text{minijet}})^\kappa}, \quad (3.4)$$

so that comparison could be made with literature [12]. The $\kappa \rightarrow 0$ limit of $Q_{\text{minijet}}(y_{\text{cut}}, \kappa)$ differs from the unweighted charge $Q_{\text{minijet}}(y_{\text{cut}})$ by a factor of track multiplicity.

Using the charge thus defined, we may further define the following quantities. First, the average minijet charge in an event is defined as:

$$\langle |Q_{\text{minijet}}(y_{\text{cut}}, \kappa)| \rangle = \frac{\sum |Q_{\text{minijet}}(y_{\text{cut}}, \kappa)|}{\#\text{minijets}}. \quad (3.5)$$

The measurement of the average minijet charge, measured and averaged over a sample of events, can confirm that charge is locally compensated. On the other hand, it would also be interesting to investigate to what extent the charge is limited to zero or ± 1 . We hence define the ratio:

$$R_{|Q|>1} = \frac{\#\text{|Q|>1}}{\#\text{minijets}}. \quad (3.6)$$

An alternative possibility would be to consider the average of some powers of minijet charge.

4. Result of simulations

We present the result of HERWIG simulations, and later provide a comparison with results obtained using PYTHIA, for the observables defined above. Unless stated otherwise, the simulations are at the hadron level and the default values in HERWIG 6.500 and PYTHIA 6.215 are adopted for the parameters affecting hadronization. The HERWIG parameters are:

$$\text{RMAS}(13) = 0.75, \quad \text{CLMAX} = 3.35, \quad \text{CLPOW} = 2.0, \quad (4.1)$$

$$\text{RMAS}(1) = \text{RMAS}(2) = 0.32, \quad (4.2)$$

$$\text{PSPLT}(1) = \text{PSPLT}(2) = 1.0, \quad (4.3)$$

$$\text{CLDIR}(1) = \text{CLDIR}(2) = 1, \quad (4.4)$$

$$\text{CLSMR}(1) = \text{CLSMR}(2) = 0. \quad (4.5)$$

Out of the parameters listed above, the most important are the following. The effective gluon mass $\text{RMAS}(13)$ (in GeV) sets the cut-off scale for the parton shower, CLMAX (in GeV) sets the maximum allowed cluster mass, and PSPLT is the power for the mass distribution in the splitting of the clusters that have masses exceeding CLMAX . The cluster mass distribution before and after the cluster splitting is shown in fig. 2. For comparison, we also show the

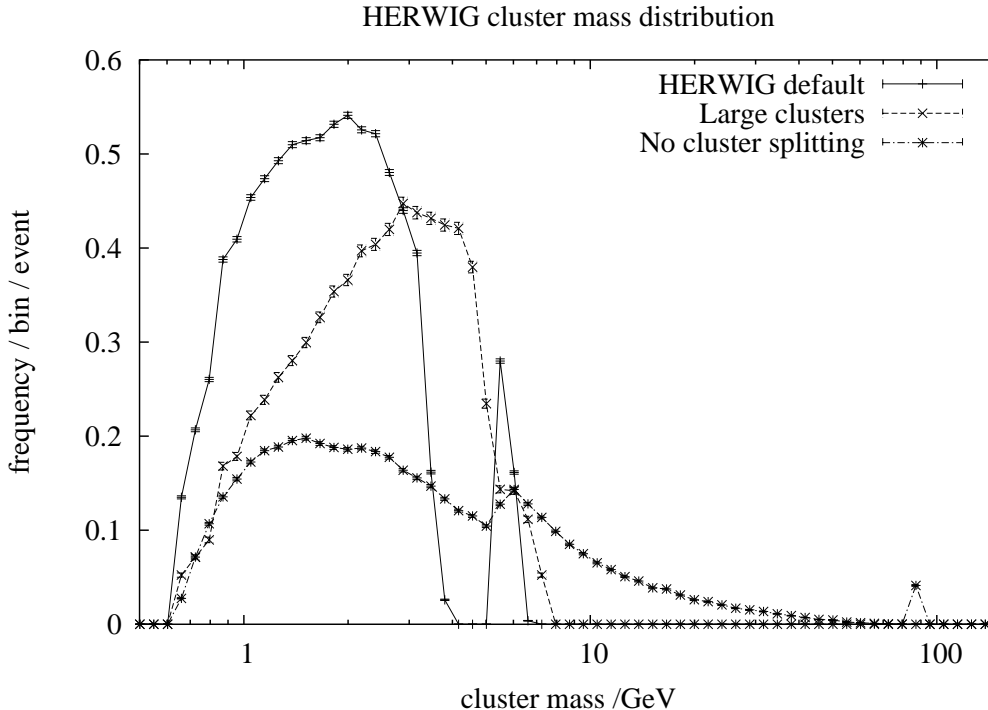


Figure 2: The HERWIG cluster mass distribution. The curve ‘HERWIG default’ is generated by the default parameter settings. The curve ‘large clusters’ corresponds to the choice $R_{\text{MASS}}(13)=1.5$ GeV, $CL_{\text{MAX}}=5$ GeV. We also show the result of having cluster splitting forbidden by setting an arbitrarily large CL_{MAX} . The peak at about 5 GeV is due to clusters containing the bottom quark.

distribution corresponding to $R_{\text{MASS}}(13)=1.5$ GeV, $CL_{\text{MAX}}=5$ GeV, which results in larger cluster masses than the default.

To clarify, when the parton shower is terminated by the effective gluon mass, clusters are first formed by splitting the gluons into $u\bar{u}$ or $d\bar{d}$. When they are heavier than approximately CL_{MAX} , clusters are split by generating an additional $u\bar{u}$ or $d\bar{d}$ pair. This is performed by uniformly generating mass raised to the power of PS_{PLT} . At the end, clusters are decayed according to the phase space weight into the available hadrons.

The other parameters, which are less important for our purpose, are the down- and up-quark masses $R_{\text{MASS}}(1)$, $R_{\text{MASS}}(2)$, the maximum cluster mass parameter CL_{POW} and the parameters CL_{DIR} and CL_{SMR} that define the extent to which the cluster decay remembers the direction of perturbatively produced quarks.

For the main part of this section, we consider the simulation of the $e^-e^+ \rightarrow q\bar{q}$ hard subprocess at the Z^0 pole, $\sqrt{s} = M_{Z^0} = 91.188$ GeV, such that $k_{T\text{cut}} = M_{Z^0}\sqrt{y_{\text{cut}}}$. Raising the energy raises the overall multiplicity and therefore raises contamination due to the misidentification of charged tracks when constructing minijets. The initial/final state photon radiation is switched off in both HERWIG and PYTHIA. There is no detector simulation. The sample size is 10000 events except where otherwise stated.

We first show the minijet multiplicity in fig. 3. Towards large y_{cut} we see that it tends

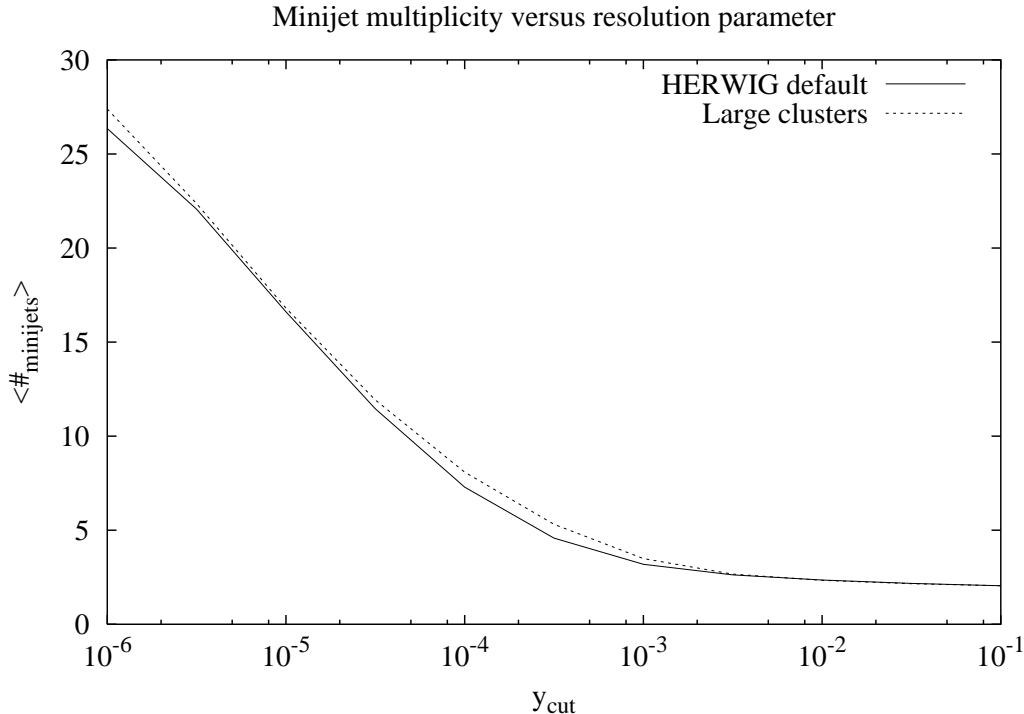


Figure 3: The minijet multiplicity plotted against the Cambridge algorithm resolution parameter y_{cut} . Sample size is 1000 events. The error due to finite statistics is small.

to 2, whereas for small y_{cut} it begins to saturate as the number of tracks is finite. A y_{cut} value of 10^{-4} corresponds to a $k_{T\text{cut}}$ of 0.91 GeV and hence of order of the cluster mass scale when using the default parameter values in HERWIG.

In the same figure, we also show the result of adopting large clusters ($\text{RMAS}(13)=1.5$ GeV, $\text{CLMAX}=5$ GeV). The difference between the two curves is slight, and the physics behind the difference is unclear. The minijet multiplicity itself is therefore not a sufficiently good observable for studying hadronization.

We now turn our attention to the average minijet charge. We carry out our simulation again for the HERWIG default and modified parameter values.

The result is shown in fig. 4. The Monte-Carlo sample size is 10000 events, but even with $\mathcal{O}(1000)$ events, the statistical error is small enough to allow comparison of the two curves. We now find that in contrast to the minijet multiplicity, we have an observable whose behaviour can be directly related to the physics of hadronization. In particular, the peak position of the average minijet charge observable, where local charge compensation is maximally violated, is close to the cluster mass scale. Far below this scale, charge becomes that of individual hadrons, whereas above this scale, local charge compensation ensures that the minijet charge does not increase arbitrarily.

Another point that is worth noting is that the minijet charge at large y_{cut} , even in the two-jet limit, is fairly sensitive to the cluster mass. If the scale of hadronization is large, minijet charge is contaminated by the reshuffling of charged tracks amongst minijets. An

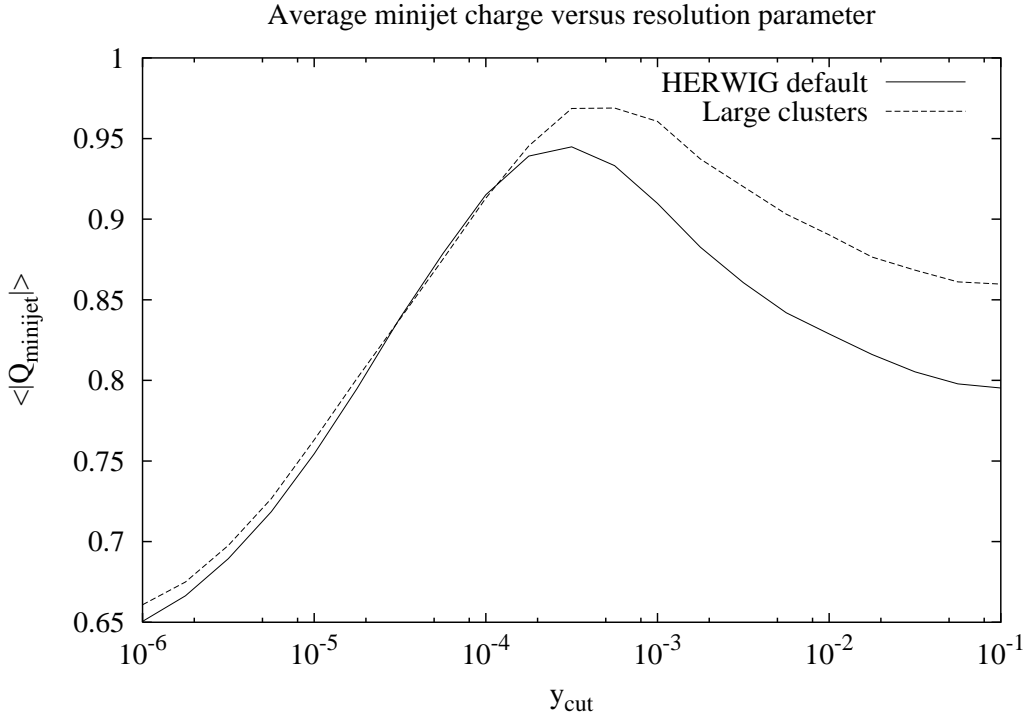


Figure 4: The mean minijet charge plotted against the Cambridge algorithm resolution parameter y_{cut} .

alternative way of seeing this is through plotting the fraction of minijets that have charge exceeding 1, as shown in fig. 5.

The relation between the minijet charge and the multiple-charge fraction can be understood as follows. Let us first consider the charge of a quark or a gluon jet in the ideal case where all clusters emitted from the originating parton is assigned to this jet. In this case, the net charge of this jet has to be equal to 0 or ± 1 with equal probability. This is because the charge is determined by the typically nonperturbative splitting $g \rightarrow q\bar{q}$ that is closest to the hard process. All other emissions conserve the jet charge. This produced quark has equal probability of being a u or a d . For the case of a quark jet, for instance, regardless of whether the originating parton is up-type or down-type, the net charge of the jet is therefore always 0 or ± 1 with equal probability. Hence the ‘perturbative’ jet charge should average to 0.5 so long as the charges of different jets are uncorrelated, or perfectly correlated in the case of the two-jet limit.

Now let us consider the contamination of this jet with at most one singly charged track, whose charge is uncorrelated with the charge of the jet, with equal probability p for each charge, $+1$ or -1 . We can show that the probabilities for the total jet charge are now modified to:

$$P_{|Q|=0} = \frac{1-2p}{2} + \frac{p}{2} = \frac{1-p}{2}, \quad (4.6)$$

$$P_{|Q|=1} = \frac{2p}{2} + \frac{1-2p}{2} = \frac{1}{2}, \quad (4.7)$$

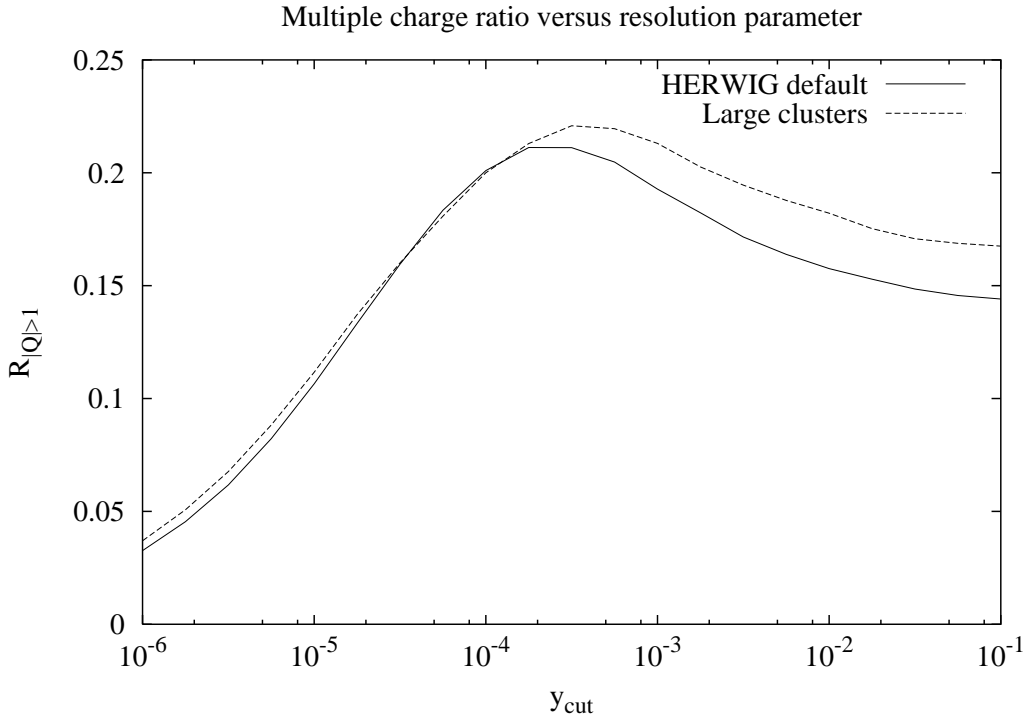


Figure 5: The fraction of minijets that have charge exceeding 1, plotted against the Cambridge algorithm resolution parameter y_{cut} .

$$P_{|Q|=2} = \frac{p}{2}. \quad (4.8)$$

Summing the charge times probability for each case, we obtain the expectation value for the net charge as $p+1/2$. On the other hand, the multiple-charge fraction is given by $P_{|Q|=2}$ above, such that we obtain the relation between the minijet charge and the multiple-charge fraction as:

$$\langle |Q_{\text{minijet}}| \rangle = \frac{1}{2} + 2R_{|Q|>1}. \quad (4.9)$$

Comparing figs. 4 and 5, we see that this relation is satisfied very well in the two-jet limit. For lower values of y_{cut} , as the nonperturbative effects become more dominant, the relation is increasingly violated, although the general behaviour is still in accord with the expectation from eqn. (4.9).

The assumption here of contamination due to at most one charged track is sufficient for our discussion, but for the sake of completeness, let us derive in outline the case without restriction on the number of uncorrelated contaminating tracks. We first define the generating function for the jet charge by:

$$\left(\frac{1}{4u} + \frac{1}{2} + \frac{u}{4} \right) \exp \left[p \left(\frac{1}{u} - 2 + u \right) \right] = \sum_{n=-\infty}^{\infty} u^n P_{Q=n}. \quad (4.10)$$

We may obtain this exponential form as the limit of binomial distribution due to infinitely many contaminating tracks, which is a direct generalization of eqns. (4.6)–(4.8). We recover eqns. (4.6)–(4.8) in the limit of small p .

Bessel functions of the first kind are defined by the generating function:

$$\exp\left[\frac{z}{2}\left(t - \frac{1}{t}\right)\right] = \sum_{n=-\infty}^{\infty} t^n J_n(z). \quad (4.11)$$

After a few elementary algebraic manipulations, we can equate the two generating functions to obtain:

$$P_{Q=n} = e^{-2p} \left[\frac{1}{4} i^{n-1} J_{n-1}(-2ip) + \frac{1}{2} i^n J_n(-2ip) + \frac{1}{4} i^{n+1} J_{n+1}(-2ip) \right]. \quad (4.12)$$

Bessel functions can be expanded in a series:

$$i^m J_m(-2ip) = \sum_{l=0}^{\infty} \frac{p^{2l+|m|}}{l!(|m|+l)!}, \quad (4.13)$$

such that corrections to eqns. (4.6)–(4.8) can be obtained systematically as an expansion in p . Furthermore, we observe that by successively operating on eqn. (4.10) by $u(d/du)$, we may obtain the expectation value for charge raised to any even integer power. For instance, operating twice with $u(d/du)$ we obtain:

$$\langle Q_{\text{minijet}}^2 \rangle = \frac{1}{2} + 2p. \quad (4.14)$$

We can estimate the contamination probability p naively as the ratio of the cluster mass against the jet energy multiplied by the cluster multiplicity:

$$p \sim \frac{M_{\text{clus}}}{\sqrt{s}/2} \times \#_{\text{clus}}. \quad (4.15)$$

The cluster multiplicity can be estimated from fig. 2. As the cluster size increases, the cluster multiplicity decreases and so there is some cancellation between the two contributions. This naive estimate can be compared with the two-jet limit of fig. 5 and we see that both the cluster mass dependence and the overall magnitude is described well. Thus the net jet charge in the two-jet limit by itself already provides a measure of the cluster mass scale.

Having said this, it is important to test to what extent the contamination is a feature of nonperturbative dynamics and not a defect of the jet algorithm, i.e., misclustering. To this effect, we repeat the analysis using different jet algorithms and show the result in fig. 6.

The JADE algorithm [11], that uses the invariant mass rather than k_T as the resolution variable, has peak at higher y_{cut} than the k_T -based algorithms. One reason is the different kinematics, namely that the k_T between two tracks is always smaller than their invariant mass. Another reason is the increased mis-clustering at high y_{cut} where the dynamics is perturbative, and reduced mis-clustering at low y_{cut} where the dynamics is nonperturbative.

Before discussing this point in more detail, we turn our attention to the three remaining, k_T -based, algorithms. The mis-clustering at moderate y_{cut} is largest for the Durham algorithm and is slightly better for the angular-ordered Durham algorithm that was mentioned in sec. 3. At very low y_{cut} , where angular-ordering is no longer a feature of the

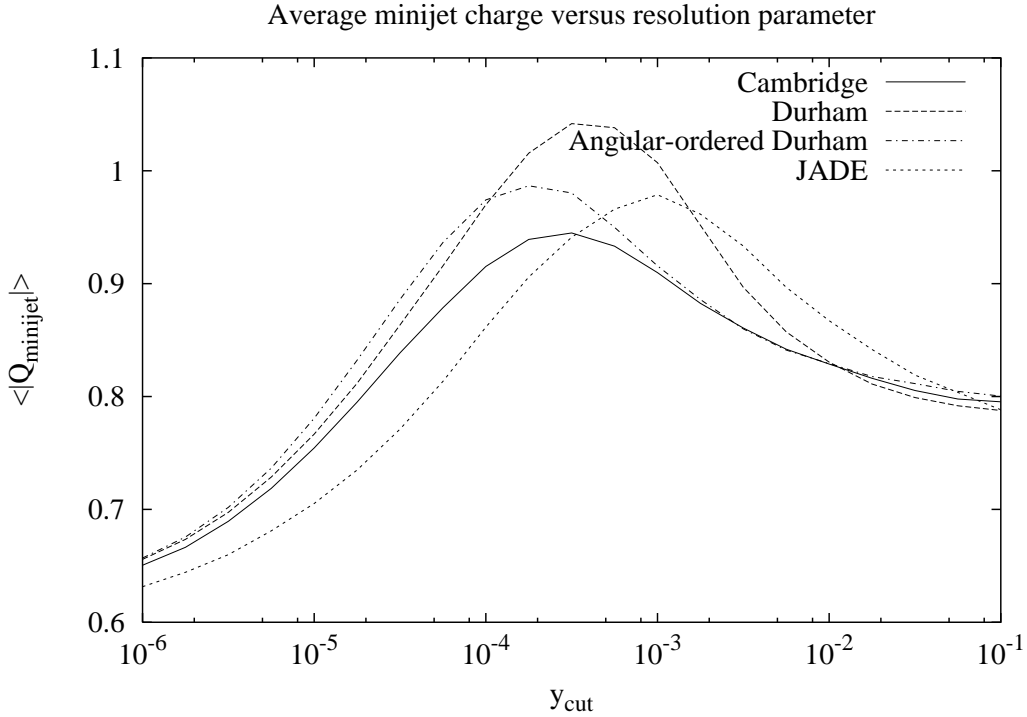


Figure 6: A comparison of the minijet charge obtained using different jet algorithms.

relevant dynamics, the Durham algorithm actually fares better than the angular-ordered algorithm.

At large y_{cut} the minijet charge due to the four algorithms converge. In particular, there is little distinction between the large y_{cut} behaviour of the Cambridge algorithm and the angular-ordered Durham algorithm from which the former algorithm is derived. Hence it seems reasonable to suppose that the minijet charge measured using the Cambridge algorithm represents the limit to which mis-clustering could be suppressed in the perturbative large y_{cut} region. In this sense, the ansatz made earlier that the contamination probability p has a mainly nonperturbative origin is reasonable.

On the other hand, towards very low y_{cut} , as we have observed above, the invariant mass, as in the JADE algorithm, may become a better resolution variable than k_T . Hence the measurement of minijet charge using these two algorithms could provide complementary information.

This suggests the introduction of a new class of scale-dependent jet algorithms, which combines the low y_{ij} behaviour of JADE with the large y_{ij} behaviour of k_T -based algorithms. As an example, we propose a ‘preclustered’ scheme, where tracks are first combined using the JADE algorithm up to some point given by the resolution parameter y_{had} , after which the tracks are combined using a k_T -based algorithm with resolution parameter y_{cut} . The case that uses the angular-ordered Durham algorithm is shown in fig. 7. The preclustering cut-off y_{had} is the normalization times $(0.5 \text{ GeV})^2$. This value is the most successful that we have been able to find when using HERWIG with default parameter values.

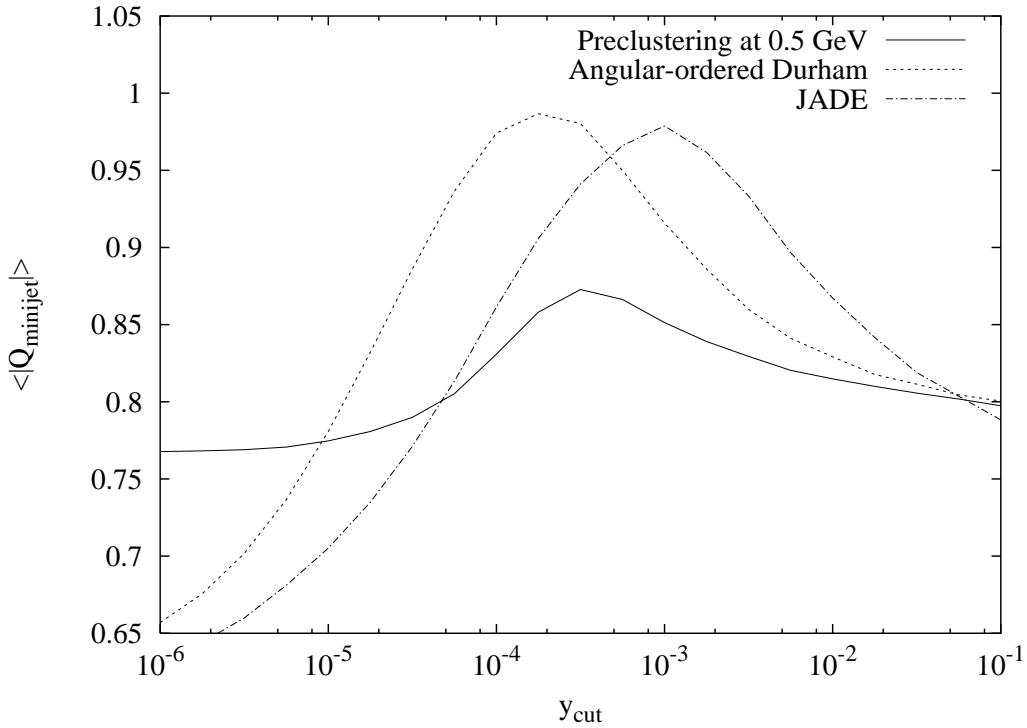


Figure 7: Minijet charge in the 0.5 GeV ‘preclustered’ angular-ordered Durham algorithm compared with the JADE and angular-ordered Durham algorithms.

There is marked improvement, in terms of the peak height and large y_{cut} behaviour, compared with either JADE or the angular-ordered Durham algorithm. There is also improvement compared with the Cambridge algorithm.

We found that there is less marked improvement when preclustering is followed by either the non-angular-ordered Durham algorithm or the Cambridge algorithm, and there is no visible improvement when the JADE preclustering phase is also angular-ordered.

The preclustered curve remains large at low y_{cut} compared with the JADE and angular-ordered Durham curves, and in the low y_{cut} limit tends to the value obtained using the JADE algorithm at the point $y_{\text{cut}} = y_{\text{had}}$.

The sensitivity of the minijet charge to the parameters affecting hadronization, as well as to the details of the jet algorithm, suggests that because of our limited knowledge about the dynamics of hadronization, the prediction of any existing Monte-Carlo event generator can not be completely trusted when charge distribution is concerned. On the other hand, the violation of local charge compensation during the hadronization phase is presumably a universal phenomenon in all models of hadronization that are based on preconfinement. Thus the general behaviour of the minijet charge observable, that peaks around the hadronization region, is a concrete prediction for this class of models.

To demonstrate this point, in fig. 8, we show the numbers obtained using PYTHIA. The overall behaviour is fairly similar, except the behaviour at very small y_{cut} , and there is an unwelcome dependence on whether the Z^0 decay is matrix-element corrected, although we

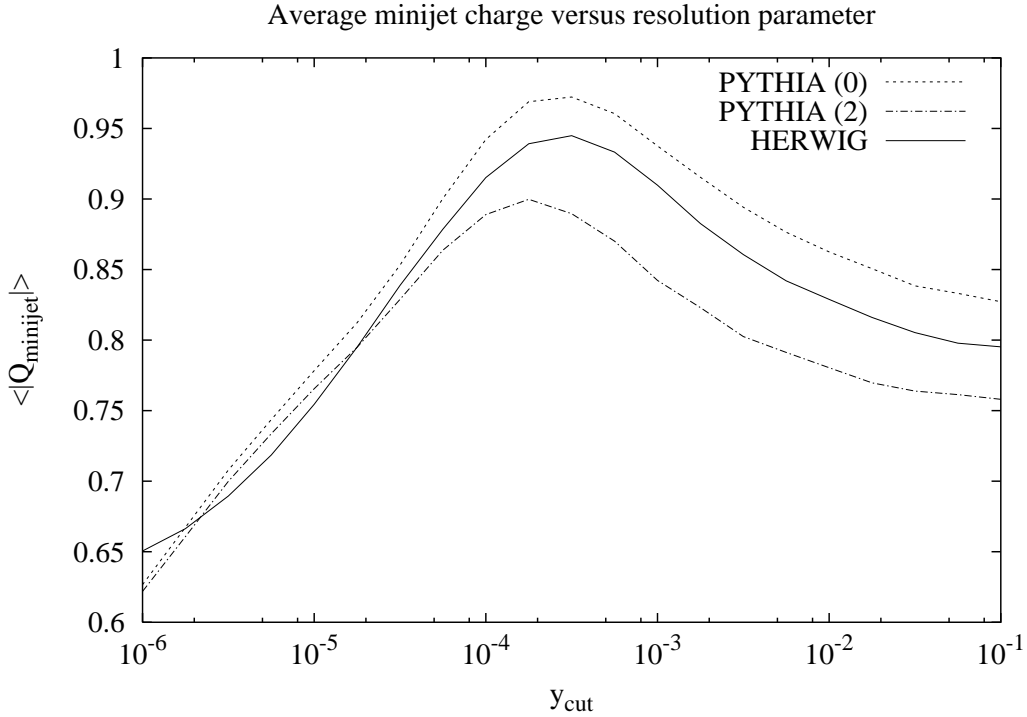


Figure 8: A comparison of HERWIG and PYTHIA for the mean minijet charge. The lines PYTHIA (0) and PYTHIA (2) correspond to the uncorrected option and the second-order matrix-element corrected option respectively for the Z^0 decay in PYTHIA.

have found that the difference between the first-order and second-order corrected options is small. We have confirmed that the corresponding difference between the matrix-element corrected and uncorrected options is almost negligible in HERWIG. The effect of adding the matrix-element correction in HERWIG is merely to raise the charge slightly at larger values of y_{cut} as expected.

As mentioned before, although the PYTHIA picture is that of string fragmentation and the mass of the string may be large to start off with, the scale at which charge is compensated is much smaller because the fragmentation proceeds by the creation of quark-antiquark pairs. We see from the figure that the peak position is roughly the same as that of HERWIG.

In fig. 9 we plot the momentum squared weighted minijet charge, which corresponds to $\kappa = 2$ in eqns. (3.4) and (3.5). The bottom quark contribution is plotted on a separate curve in order to allow comparison with ref. [12] in the two-jet (large y_{cut}) limit.

The general behaviour is quite different from the unweighted charge of fig. 4. In the low y_{cut} region, the weighted charge tends to the same value as the unweighted charge. This is interpreted as the average hadron charge. In the high y_{cut} region, the charge is much lower compared with the unweighted charge. This is because the observable suffers less from ‘contamination’ due to soft tracks.

We have also found that for a large and increasing κ ($10 \sim 50$) and in the two-jet limit,

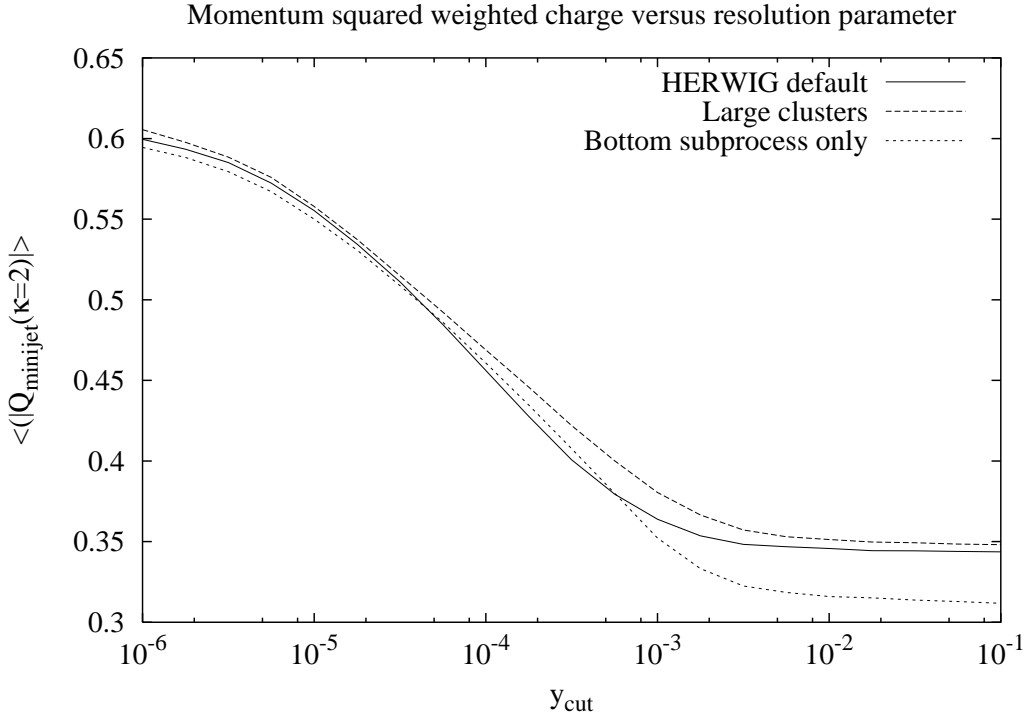


Figure 9: The momentum-squared weighted minijet charge, plotted against the Cambridge algorithm resolution parameter y_{cut} . In addition to the HERWIG default (solid line) and the large cluster (dashed line) settings, we also show the bottom quark contribution by the dotted line.

the charge slowly increases in the region $0.5 \sim 0.6$. In the limit of large κ , the momentum-weighted charge tends to the charge of the highest energy hadron in each jet. From figs. 4 and 9 we estimate the average hadron charge to be slightly above 0.6, in agreement with the above finding.

For moderate values of κ , it is not reasonable to assume that only the highest energy hadron contributes. In this case, the charge is estimated as follows. Let us assume that the highest energy hadron originates from the isotropic n -body decay of a heavier object. If this object is a cluster, n is on average ~ 4 , whereas if it is a heavy intermediate hadron, n is typically 2. It is a reasonable approximation to assume that this object has charge 0 or ± 1 , and it is also reasonable to assume that the charge of each of the decay products is also 0 or ± 1 . Then the expectation value for the momentum-weighted charge of this object, when it decays into $\#_{\text{tot}}$ objects out of which $\#_{\text{ch}}$ are charged, is simply:

$$\langle Q(\kappa) \rangle = \int_0^1 \left(\prod_{i=1}^{\#_{\text{tot}}} dz_i \right) \delta \left(\sum_{i=1}^{\#_{\text{tot}}} z_i - 1 \right) \frac{\left| \sum_{i=1}^{\#_{\text{ch}}} z_i^\kappa (-1)^i \right|}{\sum_{i=1}^{\#_{\text{tot}}} z_i^\kappa}. \quad (4.16)$$

We assumed massless kinematics. For small $\#_{\text{tot}}$ or $\#_{\text{ch}}$, this multi-dimensional integral can be evaluated analytically, but the general case is presumably best evaluated numerically.

Let us now adopt the viewpoint that the momentum-weighted charge is mainly due to the heavy intermediate hadron which decays by 2-body kinematics to give the highest

energy hadron in the jet. The other contributions are expected to mainly affect the denominator of eqn. (4.16) by increasing it, as uncorrelated contributions to the numerator cancel on average so long as they are not too large.

For the $\#_{\text{tot}} = 2$ case and $\kappa = 2$, we obtain 0, 0.5 and $\log 2 = 0.693$ respectively for $\#_{\text{ch}} = 0, 1, 2$. Disregarding the contribution from other hadrons, we can estimate the momentum-weighted charge as some weighted average of these three numbers. We note that out of the three numbers, only the $\#_{\text{tot}} = 1$ case corresponds to nonzero overall charge. Hence one possible estimate would be $0/4 + 0.5/2 + 0.693/4 = 0.42$. This is somewhat large compared with the large y_{cut} end of fig. 9, such that we see that the contribution from other hadrons is not negligible but is under control.

Our numbers for the mean momentum-weighted jet charge can be compared with the hemisphere charge separation measurement in ref. [12]. In the two-jet limit, the momentum component along the jet axis would not be very different from the momentum component along the thrust axis, such that we expect that the mean weighted charge presented here would correspond to a half of the charge separation of ref. [12]. However, a quick comparison, for example with their fig. 2, shows that there is nearly a factor of two difference. The hemisphere charge separation is much smaller than is expected from HERWIG. This may be due partly to the ‘detector effects’ included therein. Furthermore, the numbers due to JETSET presented in their tab. 4 has much greater flavour dependence than in our work, even in the $\kappa \rightarrow \infty$ limit. Further study is desired in order to elucidate the nature of the differences.

For comparison, in fig. 10, we show the result due to PYTHIA (JETSET is now part of PYTHIA). In the two-jet limit, the two generators give roughly equal numbers, such that the difference between HERWIG and ref. [12] is most likely not due to the difference in the generator. For small y_{cut} , the difference that is already visible in fig. 8 is magnified and the PYTHIA numbers show a peak at a few times 10^{-6} .

The numbers shown so far have been obtained for the simulation of e^+e^- collisions at the Z^0 pole. On the other hand, considering the high energy experiments that are currently in plan, it is interesting to consider how our procedure and results are modified for collisions in a hadron collider environment, where there are contaminations from emission near the beam axis from the initial-state parton and also from the soft underlying event.

We generate QCD $2 \rightarrow 2$ hard scattering events in $p\bar{p}$ collision at 2 TeV in the central region. We require for both outgoing partons rapidity $|y| < 0.5$ and moderate transverse momentum $30 \text{ GeV} < p_T < 50 \text{ GeV}$. Events are generated with and without soft underlying events simulated using the HERWIG default procedure and with default parameters.

Minijets are defined using the k_T -type jet algorithm of KTCLUS [13] in this case as follows. We first define macrojets by selecting a large enough y_{cut} value such that exactly two jets remain uncombined with the beam. We then construct subjets constituting these two macrojets at new values of y_{cut} . These subjets are regarded as the relevant minijets. In effect, we are studying the charge structure of tracks within the two macrojets. The normalization factor in eqn. (3.1) for y_{cut} is taken to be $1/M_{Z^0}^2$ rather than $1/E_{\text{vis}}^2$, such that the scale matches that of the e^+e^- simulations.

The result is shown in fig. 11. As the jet algorithm of KTCLUS is not angular-ordered,

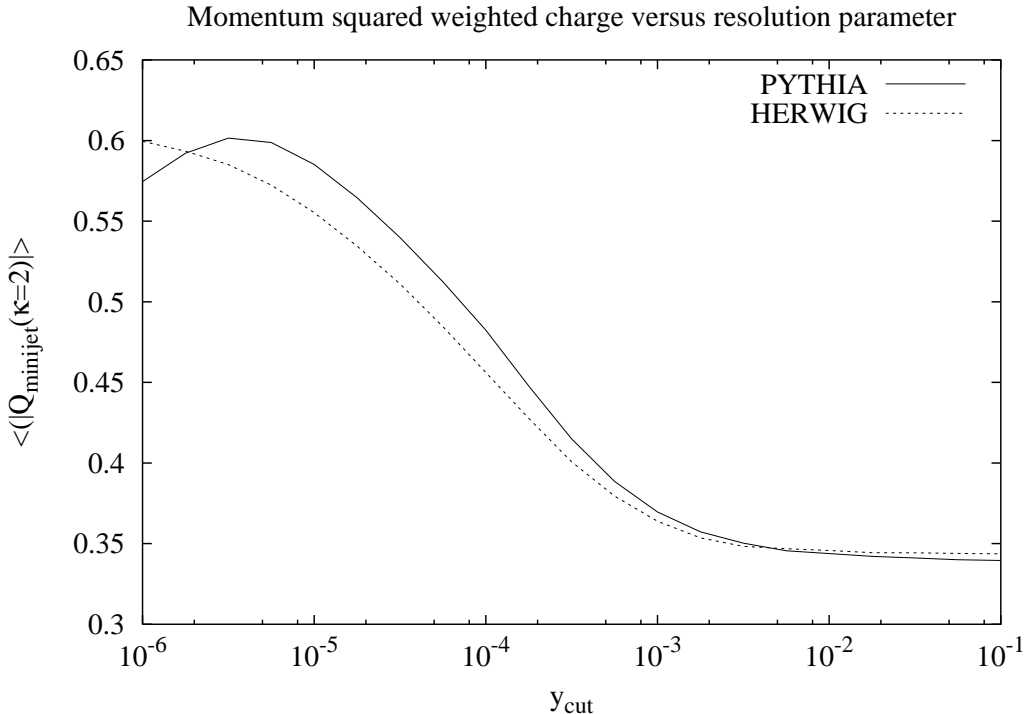


Figure 10: A comparison of HERWIG and PYTHIA for the momentum-squared weighted minijet charge. The uncorrected Z^0 decay option is adopted for PYTHIA.

we should compare the result against the Durham algorithm shown in fig. 6. When the soft underlying events are suppressed, the low y_{cut} behaviour is similar to that of fig. 6, but the peak has weakened and the minijet charge remains large at large y_{cut} . From this curve alone, it seems that the best that can be achieved in a hadron collider environment is a fit with Monte Carlo simulations. On the other hand, further refinement of the track selection procedure may improve the prospect. The additional consideration of the JADE-type algorithm is another possibility.

The effect of adding soft underlying events is quite marked. However, we note that the default procedure for soft underlying events in HERWIG violates local charge compensation such that the numbers may be regarded as a pessimistic estimate. In the alternative HERWIG-based simulations of ref. [14], as well as in PYTHIA, the underlying events are generated as multiple parton scattering and so charge is locally compensated per each scattering. Having said this, whether charge is locally compensated in soft underlying events at hadron colliders is an open question which merits further investigation.

5. Interpretation in terms of cluster dynamics

As mentioned in the previous sections, the mass of the perturbative colour-preconfined clusters is of order of the cut-off scale. Put in other words, emissions which are normally considered unresolvable in the parton shower in fact affects the mass of clusters. If so, it is perhaps natural to consider the splitting of large perturbative clusters, that occurs in

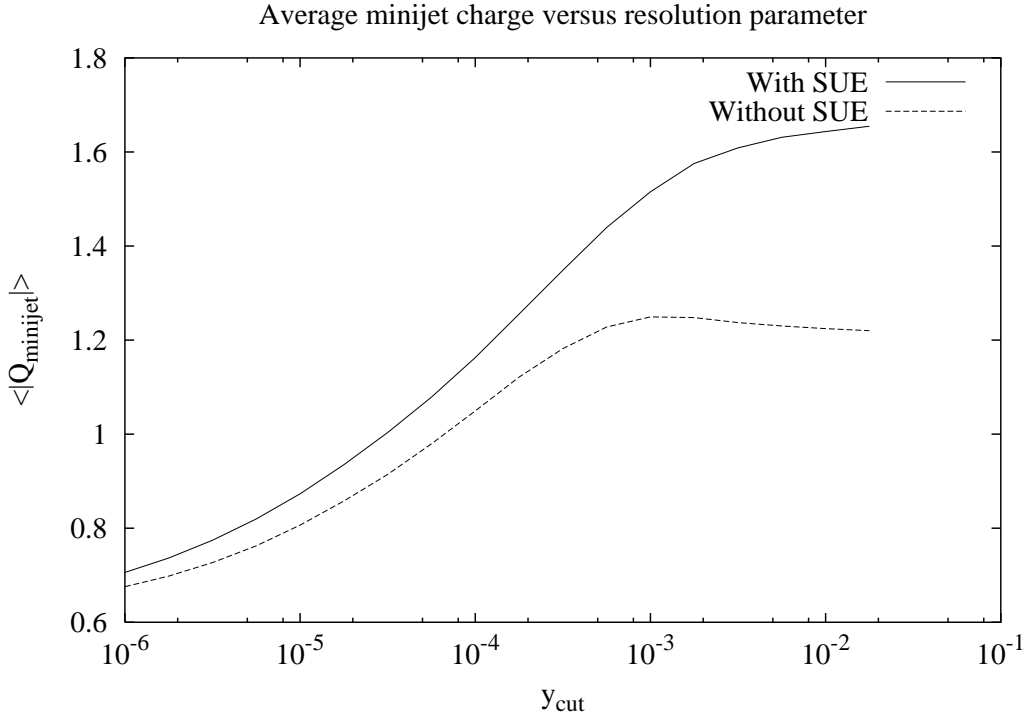


Figure 11: Minijet charge in $p\bar{p}$ collision at 2 TeV. QCD $2 \rightarrow 2$ scattering events are generated in the region $|y| < 0.5$ and $30 \text{ GeV} < p_T < 50 \text{ GeV}$, with and without soft underlying events. Only tracks belonging to the two macrojets are considered. y_{cut} is normalized by $1/M_{Z^0}^2$.

HERWIG, in terms of an extension of perturbative dynamics using a modified running α_S , which describes emission below the cut-off scale ‘before confinement’.

There are several arguments in favour of this modification. First, in the default HERWIG picture, the large clusters are split by a string-like mechanism, by creating quark-antiquark pairs in the string vacuum. On the other hand, the momentum direction of the quark and the antiquark constituting the decaying cluster is conserved as if the cluster is still an object composed of a perturbative quark and antiquark, unlike in the subsequent cluster decay which is isotropic. Second, and in principle, this substitution could lift the scale dependence in HERWIG between the parton shower phase and the cluster splitting phase such that the ambiguity due to the incomplete description of hadronization is in principle reduced to still lower scales. Third, the necessity to invoke an uncalculable string-like mechanism is removed, and we would instead have a description in terms of a modified α_S , whose properties could be subjected to further study.

Before going into a discussion of the meaning of this α_S , let us first consider the Sudakov form factor due to the left-over ‘unresolved’ emissions. The addition of an ‘unresolved’ gluon to an angular-ordered parton shower is illustrated in fig. 12, where we consider the emission of an unresolved gluon in between rapidities y_0 and y_1 , where y_0 and y_1 are the rapidities of the gluons which have been emitted in the course of the resolved parton shower.

The emission probability of a gluon in a phase space element (dQ^2, dy) , where Q^2 and

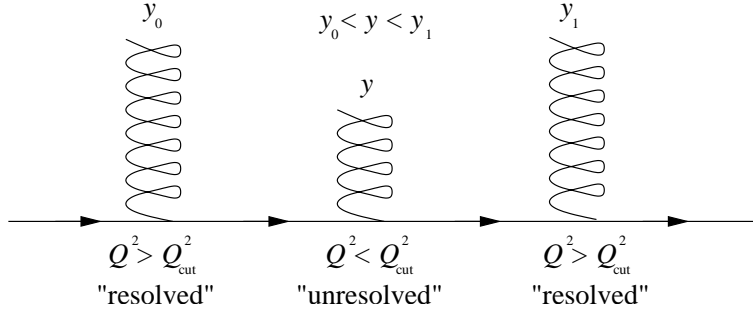


Figure 12: The addition of an ‘unresolved’ gluon to an angular-ordered parton shower in between colour connected partons (gluons). y is the rapidity of the emitted parton.

y are the p_T^2 and rapidity of the emitted gluon respectively, in the soft limit, is:

$$dP_{\text{emission}} = \frac{dQ^2}{Q^2} dy \frac{\alpha_S(Q^2)C}{\pi} \quad (5.1)$$

The colour factor C is C_F for emission from a quark and C_A for emission from a gluon. As we are considering cluster dynamics and the gluon is effectively a quark–antiquark object in this respect, the colour factor is C_F , or equally well $C_A/2$, at leading order in $1/N_C$.

The equivalence of this expression with the ordinary angular-ordered parton shower [16] in the soft limit is demonstrated as follows. Let us consider the emission probability from a quark in the splitting $q_a \rightarrow q_b g_c$:

$$dP_{\text{emission}}(q_a \rightarrow q_b g_c) = \frac{d\tilde{t}}{\tilde{t}} \frac{dz_b}{2\pi} \alpha_S(Q^2) \hat{P}_{qq}(z_b). \quad (5.2)$$

Here $\tilde{t} = E_a^2(1 - \cos\theta_{bc})$. E_a is constant until an emission takes place, such that $d\tilde{t}/\tilde{t} = d\theta^2/\theta^2 = 2dy$ in the soft and the usual small angle limit. In the soft limit, the splitting function $\hat{P}_{qq}(z_b) = 2C_F/z_c$, such that we have:

$$dP_{\text{emission}}(q_a \rightarrow q_b g_c) = 2dy \frac{dz_b}{2\pi} \alpha_S(Q^2) \frac{2C_F}{z_c}. \quad (5.3)$$

Now replacing dz_b by dz_c and using $Q^2 = 2\tilde{t}z_c^2$ in the soft limit, we see that the two expressions are equivalent.

For an angular-ordered parton shower, the emission is ordered in y . The Sudakov form factor is:

$$\Delta_q(y) = \exp \left[- \int \frac{dQ^2}{Q^2} dy \frac{\alpha_S(Q^2)C_F}{\pi} \right]. \quad (5.4)$$

We are only interested in emission below the cut-off scale, such that the Q^2 integration factorizes out:

$$\Delta_q(y) = [\exp(y - y_0)]^{-I_0}, \quad (5.5)$$

where

$$I_0 = \int_0^{Q_{\text{cut}}^2} \frac{dQ^2}{Q^2} \frac{\alpha_S(Q^2)C_F}{\pi}. \quad (5.6)$$

The integral is finite if α_S tends to zero as a power as Q^2 tends to zero. A possible physical argument would be to say that if colour is confined in the large distance limit, then any α_S with some physical interpretation as the coupling of coloured objects can be defined to vanish as a power.

We may thence carry on to estimating I_0 in the above using models of low energy α_S . As an example, and not necessarily an appropriate one, we may consider the effective α_S of ref. [15], which is derived from the general consideration of power-suppressed corrections to event-shape observables. In this approach, the renormalon chain which gives rise to the power-suppressed corrections is summed using a dispersion relation. The effective α_S is defined to be analytic everywhere except along the negative real Q^2 axis, and its infrared behaviour is connected to the power corrections through the analyticity of the observable under attention, or more precisely its characteristic function, as a function of small squared ‘gluon mass’.

One difficulty when using this α_S to estimate I_0 is that it remains finite as $Q^2 \rightarrow 0$ as shown in fig. 13, such that its integral is not finite. In the dispersive resummation of the renormalon chain, this is not a problem as only the moments of α_S are related to the power-suppressed corrections. For now we content ourselves by cutting off at $Q \sim 0.1$ GeV and integrating up to the HERWIG cut-off at around $\text{RMAS}(13)=0.75$ GeV. We obtain $I_0 \sim 1$.

We shall discuss the above points regarding the behaviour of low-energy α_S in more detail in sec. 6.

It is a simple matter to relate the emission dynamics to the kinematics of cluster splitting. Let us consider the splitting of a dipole with mass M_0 into two smaller dipoles with masses M_1 and M_2 . The kinematics has already been calculated in the context of the dipole cascade formalism in ref. [17]. As the integral is Lorentz invariant, let us transform to the cluster frame. Neglecting quark masses, rapidity in this case is:

$$y = \log(M_2/M_1), \quad (5.7)$$

$$|y| \lesssim \log(M_0/Q_{\text{cut}}). \quad (5.8)$$

Combining these with eqn. (5.5) and $I_0 \sim 1$, we may estimate the probability of there being no splitting. If the cluster mass is ten times greater than the cut-off, for example, the probability of the cluster surviving without emission is only 1%.

In general, as can be inferred from eqns. (5.5) and (5.8), I_0 governs the average number of smaller clusters that a large cluster splits into, viz.:

$$\langle \#_{\text{split}} \rangle \sim I_0 \Delta y \approx I_0 \log \frac{M_0^2}{Q_{\text{cut}}^2}. \quad (5.9)$$

From fig. 2, we can estimate the value of $\langle \#_{\text{split}} \rangle$ that leads to the correct cluster multiplicity. We estimate this number to be ~ 3 and M_0 to be ~ 10 GeV. This gives $I_0 \sim 0.5$ and thus $I_0 \sim 1$ obtained above is too large.

$Q^2 = p_T^2$ on the other hand controls the typical cluster mass, and can be expressed as:

$$Q^2 = \frac{M_1^2 M_2^2}{M_0^2}. \quad (5.10)$$

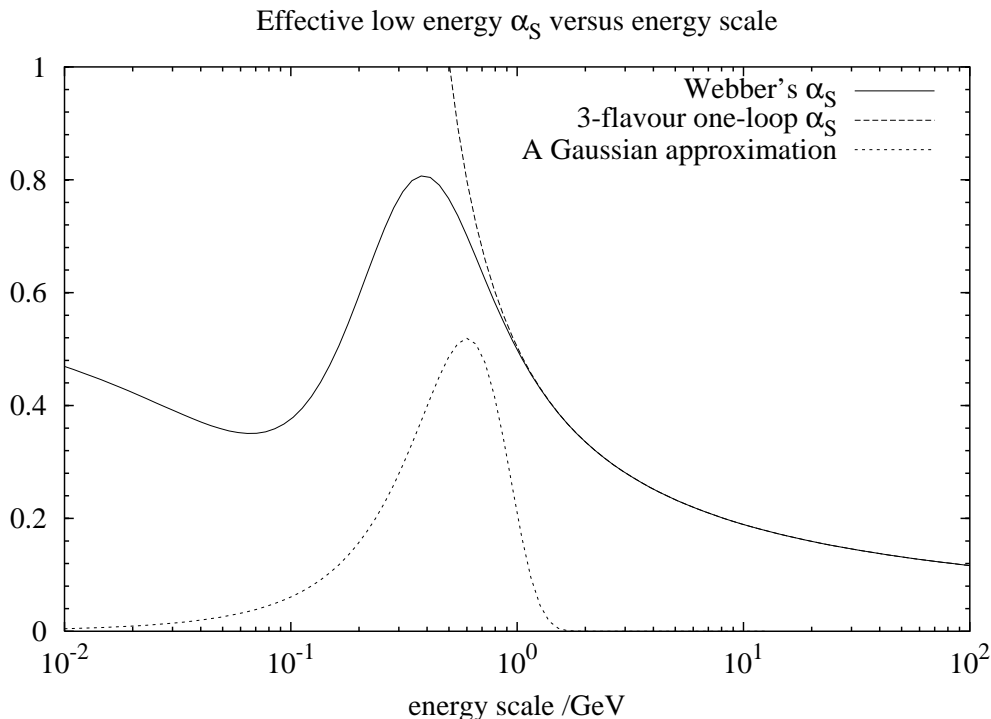


Figure 13: The effective α_S of ref. [15], derived from the general consideration of power-suppressed corrections to event-shape observables. The effective α_S coincides with the three-flavour α_S in the high-energy limit. The three-flavour Λ_{QCD} is taken to be 0.25 GeV. We also show a Gaussian approximation, with arbitrary normalization.

If we omit the consideration of the nonperturbative $g \rightarrow q\bar{q}$ splitting that converts the dipoles into clusters, the physics of which we do not yet understand and which we will discuss in sec. 6, the cluster splitting is henceforth governed by the above equations. One should add a technical detail, that in HERWIG, the cluster mass that is considered has the constituent quark masses subtracted.

We note that the default cluster splitting procedure of HERWIG violates the above expression, eqn. (5.10), for Q^2 , when the product of the masses of the two decay products divided by the decaying cluster mass is greater than the parton shower cut-off.

Based on the above considerations, we carry on to creating a simple code which modifies HERWIG to perform cluster decay by the modified- α_S approach. However, there are two subtleties that need to be dealt with.

First, if there is a cascade splitting of clusters, one must be careful not to double-count soft emission. The simplest method for avoiding double-counting would be to introduce a flag. On the other hand, when making a HERWIG implementation, as there is a cut-off on the maximum allowed cluster mass, this problem is not severe.

Let us consider again the cluster mass distribution shown in fig. 2. The parton shower cut-off, which also signifies the scale of the low-energy cluster-splitting dynamics, is of order $\text{RMASS}(13)=0.75$ GeV, whereas the minimum cluster mass that is split is around

CLMAX=3.35 GeV. We see that in most of the cases, provided that eqn. (5.10) is satisfied, at least one of the decay products is lighter than the cut-off. Hence there would be no further emission from this lighter cluster, and by adopting an ordering that starts from the largest value of $|y|$, the problem would be resolved.

Second, and related to the first point, the ordering in y is not strictly necessary. So long as the cluster mass can be considered large compared with the parton shower cut-off, the order in which the ‘unresolved’ gluons are emitted, in principle, does not matter. However, in a practical HERWIG implementation, because of the cut-off on the maximum allowed cluster mass and the incomplete description of physics below this scale, there does remain some dependence on the ordering.

In particular, when using the above effective α_S , because $I_0 \sim 1$ is large, we have found that if emission is in the order of decreasing $|y|$ as suggested above, too many clusters are formed with small mass. This is unwelcome in the sense that these small clusters can not be considered perturbative objects. On the other hand, when $I_0 \sim 0.5$ as is preferred from multiplicity considerations, we have found that there is not much dependence on whether $|y|$ is ordered. In this case there is not a clear-cut connection between the presence of this ordering and, for example, the cluster mass distribution, such that for now, we may abandon the ordering in y and generate it uniformly.

After the above considerations, we implement the following procedure, which is not precisely the procedure dictated by the modified- α_S approach, but more close to the HERWIG default cluster-splitting algorithm:

1. Terminate the parton shower by means of an artificial gluon mass `RMASS(13)=0.75` GeV, as according to the HERWIG default prescription.
2. For clusters whose mass is greater than about CLMAX, or more precisely for a cluster with mass M made from quarks i and j :

$$M^{\text{CLPOW}} > \text{CLMAX}^{\text{CLPOW}} + (\text{RMASS}(i) + \text{RMASS}(j))^{\text{CLPOW}}, \quad (5.11)$$

split the cluster, as follows.

3. Rapidity is first generated, not by following eqn. (5.5), but as a flat distribution in the range suggested by eqn. (5.8). This is correct in the limit where there is one and only one ‘unresolved’ emission. It is also correct in the case where emission is ordered in Q^2 , as in ref. [17]. In this case, the distribution of Q^2 described below should be interpreted as a Sudakov form factor rather than α_S .
4. Q^2 is generated in between the parton shower cut-off scale and the lower cut-off scale for α_S , according to the distribution:

$$\propto \frac{dQ^2}{Q^2} \alpha_S(Q^2). \quad (5.12)$$

5. The process is repeated until there remains no more cluster that satisfies eqn. (5.11). Thus all clusters above the cluster-mass cut-off are split. The error due to disallowing some heavy clusters is negligible so long as the probability of splitting, or the parameter I_0 , is sufficiently large.

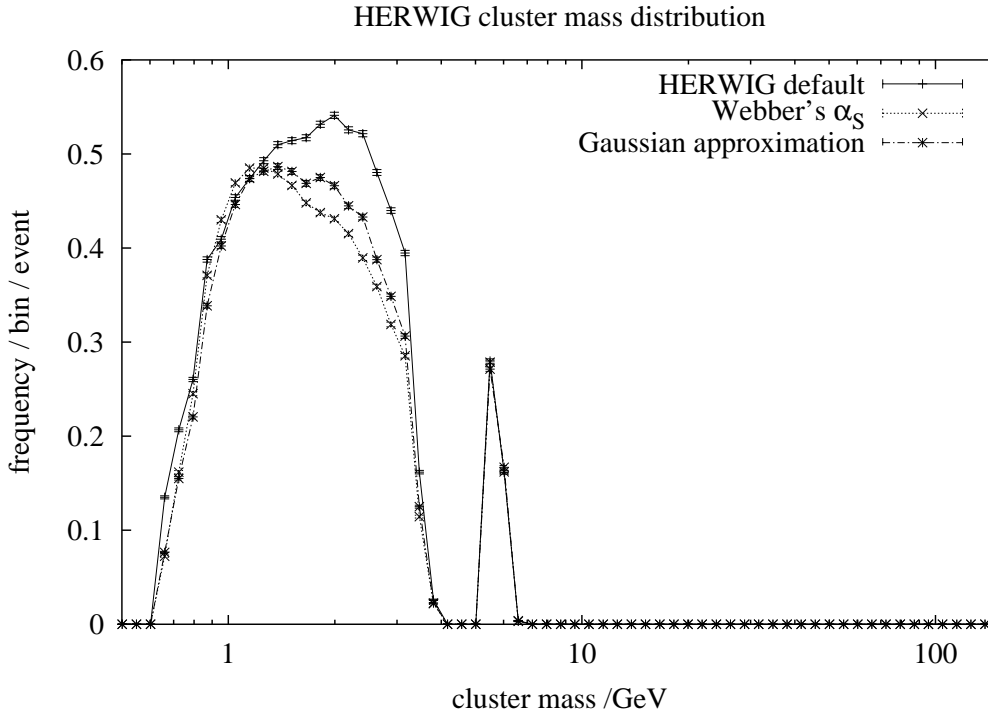


Figure 14: The cluster mass distribution generated using the HERWIG default procedure, the α_S of ref. [15] and a Gaussian approximation with $Q_{\min} = 0.1$ GeV.

In the above implementation, the normalization of α_S , which should affect multiplicity, is nevertheless irrelevant so long as we abandon y ordering. Hence one may as well substitute for low energy α_S by a Gaussian distribution. A useful substitution may be:

$$\propto Q \exp \left[\frac{(Q - Q_{\text{mean}})^2}{2(\Delta Q)^2} \right], \quad (5.13)$$

such that Q is generated with mean Q_{mean} and standard deviation ΔQ . Although this is a fairly economical parametrization, we may further reduce the number of parameters by setting the upper limit equal to the parton-shower cut-off. Thus we set:

$$Q_{\text{mean}} = \frac{\text{RMAS}(13) + Q_{\min}}{2}, \quad (5.14)$$

$$\Delta Q = \frac{\text{RMAS}(13) - Q_{\min}}{2}. \quad (5.15)$$

The Gaussian distribution corresponding to $Q_{\min} = 0.1$ GeV is shown in fig. 13.

The cluster mass distribution due to this choice is shown in fig. 14, where we compare it against the HERWIG default distribution and against the result of adopting the procedure above with the α_S of ref. [15]. When using this α_S , Q^2 is generated in between 0.1 GeV and 0.75 GeV.

We see that with $Q_{\min} = 0.1$ GeV, although the distribution is close to the HERWIG default, the distribution is too skewed to the low mass end, and multiplicity is not large

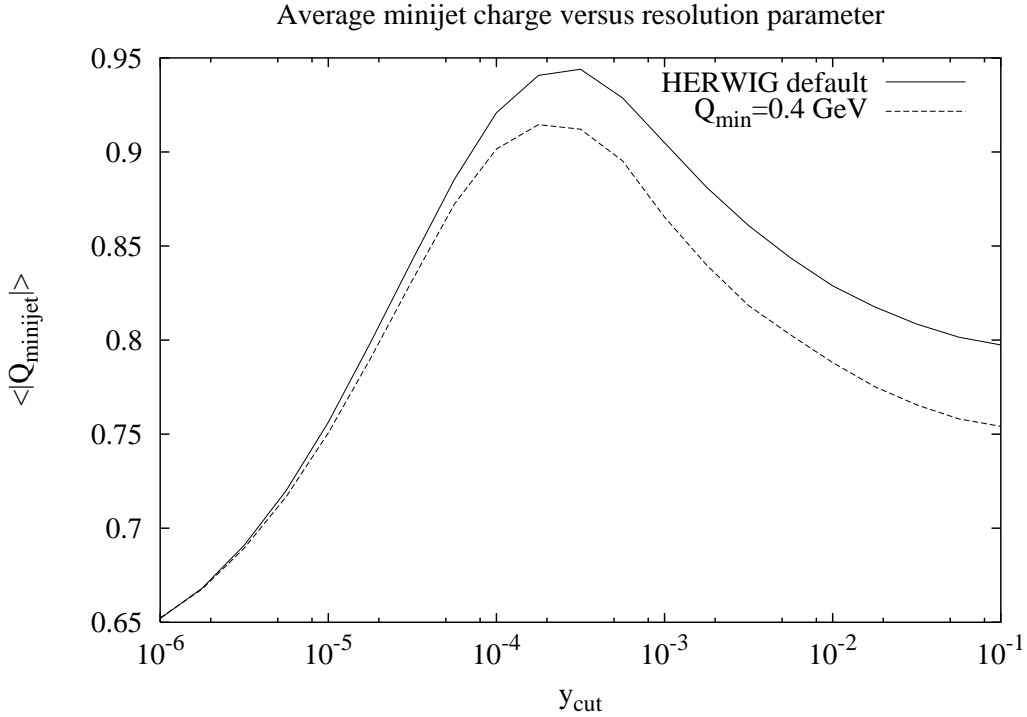


Figure 15: The mean minijet charge plotted against the Cambridge algorithm resolution parameter y_{cut} . The sample size is 50000 events for each curve.

enough. These two problems are mutually related, but presumably the more serious is the skew to the low-mass end, as the multiplicity is in principle affected by the normalization of α_S as noted above.

Both problems can be rectified by raising Q_{min} , and we have found that the correct enhancement of the high mass end is obtained at $Q_{\text{min}} \sim 0.4 \text{ GeV}$. The individual identified particle yields are also affected by this cluster mass distribution. As the shape of the distribution is not identical with the HERWIG default, the yields would be slightly different, but as there is no reason to believe that the Gaussian distribution resembles reality, there would be no reason to believe that the resulting yields would be closer or farther to reality than the default HERWIG numbers.

In fig. 15, we show the average minijet charge. The numbers are stable with respect to small perturbation of the parameter Q_{min} . The result shows that the peak position in y_{cut} has shifted slightly to the left compared to the HERWIG default numbers, and the peak height is smaller. As the cluster mass distribution itself is more or less unchanged, this modification should be interpreted as the result of having less probability of a large cluster splitting into two adjacent large clusters. Thus a modification of HERWIG that excludes cluster splitting that can be interpreted as due to high p_T emission leads to the suppression of minijet charge.

This argument also helps to understand why the PYTHIA minijet charge, without the matrix element correction, is larger than the HERWIG result, as seen in fig. 8.

It is interesting to see whether event shape observables are also affected. We have computed sphericity and found that the modification due to the implementation of the new algorithm is slight.

6. Interpretation of low energy α_S

What we have learnt from the above simulation in terms of the dynamics of hadronization is that the scale relevant to the splitting of clusters is between about 0.4 GeV and 0.75 GeV. In terms of the perturbative α_S , between about 0.5 and 1.

What remains is to understand the origin of this structure. If we reduce the scale of splitting, the cluster mass distribution is too skewed towards the low mass end and multiplicity becomes insufficient. It would not be sufficient to propose, for instance, that only the highest p_T emission affects the splitting of clusters.

Let us consider a toy model, in which perturbative emissions have Sudakov form factor $\Delta(Q^2)$ and the confinement interaction has Sudakov form factor $\Delta_C(Q^2)$. Then the probability of emission ‘before confinement’ is given by exponentiating the emission probability times the survival probability and hence the following modified Sudakov form factor:

$$\Delta_{\text{effective}}(Q^2) = \exp \left[\int \frac{dQ^2}{Q^2} \Delta_C(Q^2) \frac{d \log \Delta(Q^2)}{dQ^2} \right] \quad (6.1)$$

$$= \exp \left[- \int \frac{dQ^2}{Q^2} dy \Delta_C(Q^2) \frac{\alpha_S(Q^2) C_F}{\pi} \right]. \quad (6.2)$$

Although the confining potential is not obtained at any finite order of perturbation theory, for the sake of discussion we may write confinement as an $\mathcal{O}(\alpha_S^2)$ ‘gluon exchange’ process. Thus $\Delta_C(Q^2) = 1 - \mathcal{O}(\alpha_S^2)$ and hence we have a plausible explanation for the suppression of emission at lower scales where $\alpha_S(Q^2)$ becomes large.

In terms of probability, this is equivalent to saying that although the emission of gluons at low Q^2 has large probability, in the time that it takes to have this emission, there is greater probability that the cluster will be confined. Hence emission is suppressed.

In terms of effective α_S , the effective α_S that controls ‘unresolved’ emission that splits the cluster is expanded in terms of perturbative α_S as $\alpha_S - \mathcal{O}(\alpha_S^3)$. However, the coefficient may depend on the cluster mass and the nature of the observable and hence this α_S is not necessarily universal.

In the above model, we have assumed that the onset of confinement is sudden. This is also the case in HERWIG, where the ‘confined’, ‘nonperturbative’ clusters thus formed then decay isotropically. In reality, the soft gluon exchange interaction between the quark and the antiquark in a cluster is expected to enter earlier. Hence clusters would be ‘rotated’ as illustrated in fig. 16. We expect that this leads to the broadening of the peak in the minijet charge observable, although a quantitative prediction is beyond the scope of this study.

Let us illustrate and concretize the above discussion of ‘emission before confinement’ by considering the dynamics of the $g \rightarrow q\bar{q}$ splitting intrinsic to HERWIG which is not understood. If this splitting is physical, for instance if confinement enhances this splitting,

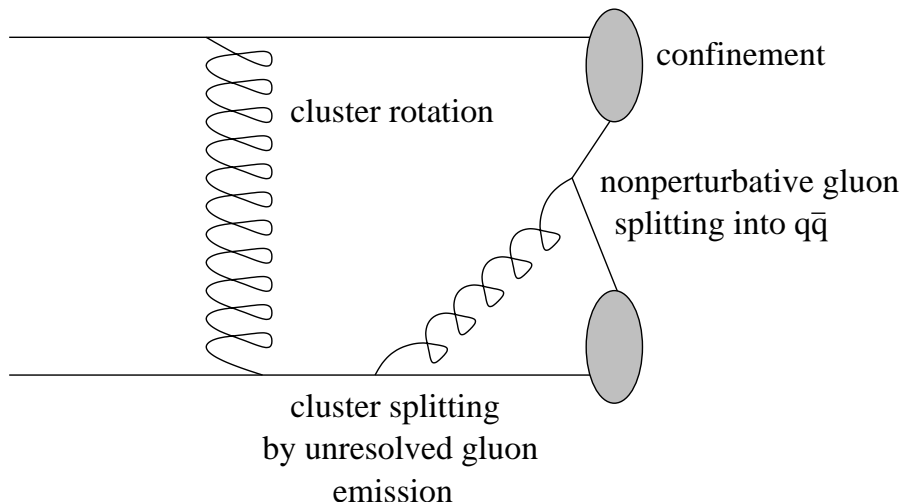


Figure 16: Perturbative and nonperturbative dynamics affecting perturbative clusters.

it would be possible to define the corresponding beta function. Solving the renormalization group equation, we may define another α_S that may be regular in the infrared. This provides another viewpoint that is compatible with the above toy model in the sense that we may loosely identify ‘confinement’ with the $g \rightarrow q\bar{q}$ splitting.

We may define the effective strength for gluon splitting, that could be used to replace HERWIG’s non-perturbative gluon-splitting, as follows:

$$T_{\text{eff}}(Q^2) = \frac{11C_A}{4} - 3\pi\beta(Q^2), \quad (6.3)$$

where $\beta = d\alpha_S^{-1}/d\log Q^2$. $T_{\text{eff}} = n_f T_R$ in perturbation theory at the lowest order, but it becomes large at low scales for any parametrization of α_S that turns over. If we require that α_S vanishes as a power of Q^2 such that its integral with respect to $\log Q^2$ is finite, we see that T_{eff} must diverge towards $Q^2 \rightarrow 0$ with the same power, i.e., $\alpha_S T_{\text{eff}}$ tends to a constant. Although this power behaviour can not be obtained at any finite order in perturbation theory, it is precisely what one would expect as the form of a nonperturbative higher-twist contribution. We may write:

$$\beta(Q^2) = \beta_{\text{pert.}}(\alpha_S) - \frac{A}{Q^n}. \quad (6.4)$$

Dropping the higher order perturbative contributions, we obtain α_S as:

$$\alpha_S(Q^2) = \frac{1}{\beta_0 \log(Q^2/\Lambda^2) + 2A/(nQ^n)}. \quad (6.5)$$

Here $\beta_0 = (33 - 2n_f)/12\pi$. Although the forced $g \rightarrow q\bar{q}$ splitting in HERWIG only involves two flavours, for the sake of consistency with the previous discussions, let us adopt $n_f = 3$ for now. This α_S has the desired properties of integrability under $\log Q^2$ and remaining well-defined on the positive real axis, provided that $A > \beta_0 \Lambda^n e^{-1}$ such that the denominator is positive definite. On the other hand, when either the denominator is positive definite or $n > 4$, the expression has complex poles.

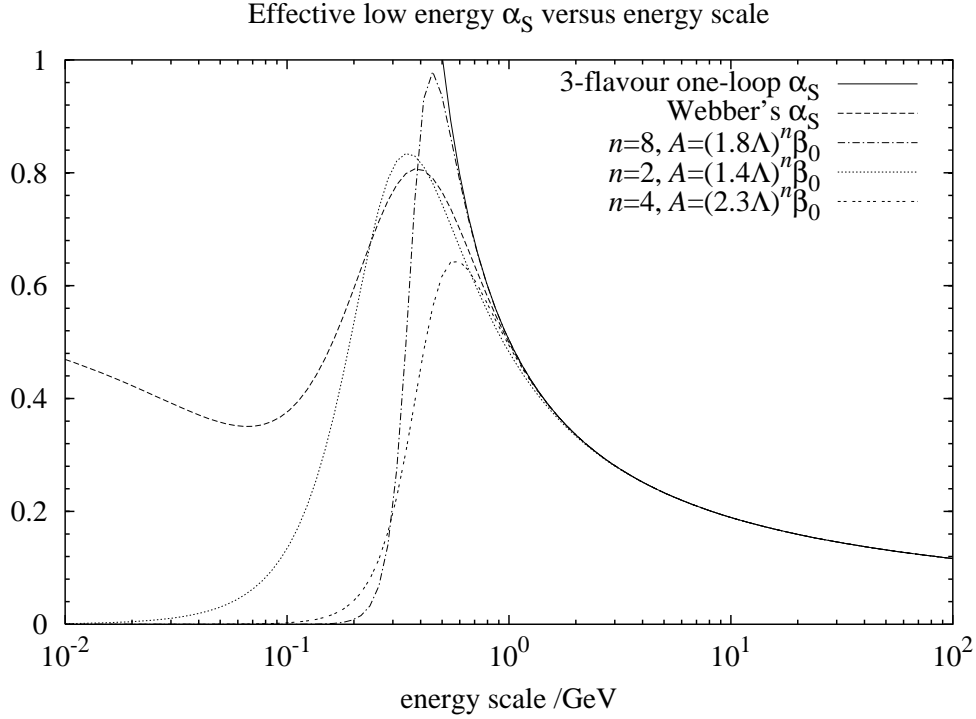


Figure 17: The α_S derived from a power corrected beta function.

If we require that this α_S is universal, we should require that n is large such that we do not introduce power corrections that are not predicted by the OPE formalism to quantities that are proportional to $\alpha_S(Q^2)$ in leading order such as the e^+e^- total cross section. OPE predicts a term proportional to the dimension-4 gluon condensate, which is therefore $\propto 1/Q^4$ by dimensional analysis, whereas the above α_S gives rise to terms $\propto (\alpha_S^{\text{PT}})^2/Q^n$ for large Q , where α_S^{PT} is the perturbative α_S , such that the $n = 2$ case is forbidden.

In the discussion of ref. [18], even additional contributions proportional to $1/Q^4$ is disfavoured, as this gives an additional ‘nonperturbative’ contribution which is not related to the region of small momentum flow, i.e. the region which is responsible for the condensates that give rise to the power corrections, in the corresponding Feynman diagrams.

As an example, let us adopt $n = 8$ here, which is the same as the large Q^2 behaviour of the effective α_S of ref. [15]. We set $A = (1.8\Lambda)^n \beta_0$ and display the behaviour of this particular choice in fig. 17. For reasonable choices of the parameter A , the low energy cut-off is large, in quantitative agreement with our earlier finding that $Q_{\text{min}} \sim 0.4$. On the other hand, the low Q^2 behaviour of the aforementioned α_S is matched better for small n . In fig. 17, we also plot the $n = 2$ case for comparison, with $A = (1.4\Lambda)^n \beta_0$.

As stated above, the $n = 2$ case is forbidden and a $1/Q^4$ correction is disfavoured by OPE, but we claim that this argument does not apply to our α_S at $n = 4$, since what we are considering is a possibly universal correction to α_S arising from OPE, which therefore arises from the region of small momentum flow.

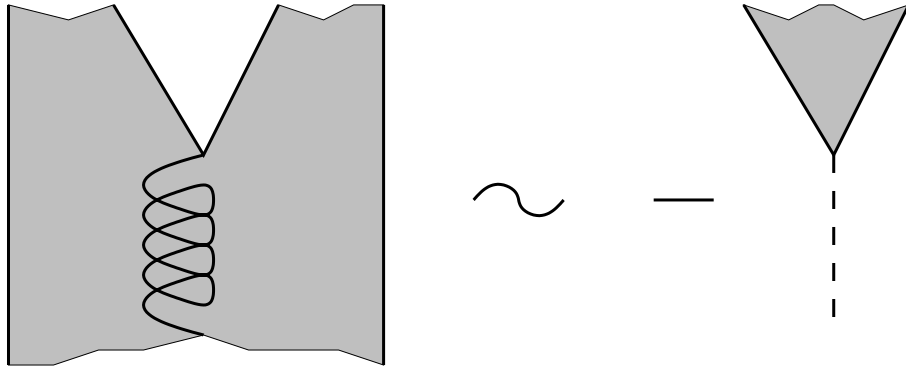


Figure 18: An illustration of the splitting of a ‘kinked string’ by the parton splitting $g \rightarrow q\bar{q}$. Classically, the string ‘pulling apart’ the quark and antiquark approximates to a string with negative tension ‘pushing apart’ the partons.

If the $g \rightarrow q\bar{q}$ splitting is indeed enhanced by confinement, an intuitively appealing picture would be that the quark and the antiquark are ‘pulled apart’ by the large-distance string-like confining potential, as shown in fig. 18. This would classically approximate to a string with negative tension ‘pushing apart’ the quark and the antiquark, and hence by dimensional analysis the contribution to the effective strength for gluon splitting is expected to be:

$$T_{\text{eff}} = n_f T_R \left[1 + \mathcal{O}(\alpha_S) + \mathcal{O}\left(\frac{\sigma^2}{Q^4}\right) \right]. \quad (6.6)$$

$n_f T_R = 1$ or 1.5 depending on whether the splitting $g \rightarrow s\bar{s}$ is allowed. Hence $A \sim \sigma^2$. Let us test the validity of this parameter choice. First, the peak position in this α_S is given by the point at which the beta function vanishes in eqn. (6.4), i.e.:

$$A = \beta_0 Q_{\text{peak}}^n. \quad (6.7)$$

Now from eqn. (5.14) and $Q_{\text{min}} = 0.4$ GeV, $Q_{\text{peak}} = 0.575$ GeV. Thus $A = \beta_0 Q_{\text{peak}}^2 = 0.237$ GeV² is in good agreement with what one might expect for the string tension $\sigma \sim 0.2$ GeV² [19]. The corresponding α_S is shown in fig. 17.

The area underneath α_S and hence I_0 in eqn. (5.5) can be calculated numerically. For $A = (2.3\Lambda)^n \beta_0$ where $\Lambda = 0.25$ GeV such that $Q_{\text{peak}} = 0.575$ GeV, and integrating up to 0.75 GeV, we obtain $I_0 = 0.536, 0.441, 0.389$ and 0.355 for $n = 2, 4, 6$ and 8 respectively. From multiplicity considerations the preferred value is $I_0 \sim 0.5$ according to the estimation from eqn. (5.9), such that the values are reasonable, though the $n = 6$ and 8 cases are possibly too small.

The cluster mass distribution corresponding to $n = 2, 4$ and 8 are shown in fig. 19. At first sight, it seems that the $n = 8$ distribution matches the HERWIG default numbers best, hence implying that the low-energy tail of the α_S for $n = 4$, or 2 , is too high. On the other hand, if the tail is not sufficiently high, as in the $n = 8$ case, there would not be sufficient contribution to I_0 . Hence there seems to be a contradiction here. However, one reason why the Gaussian approximation in eqn. (5.13) can rectify the small-mass oriented skew of the cluster mass distribution is that there is some contribution from Q^2 above

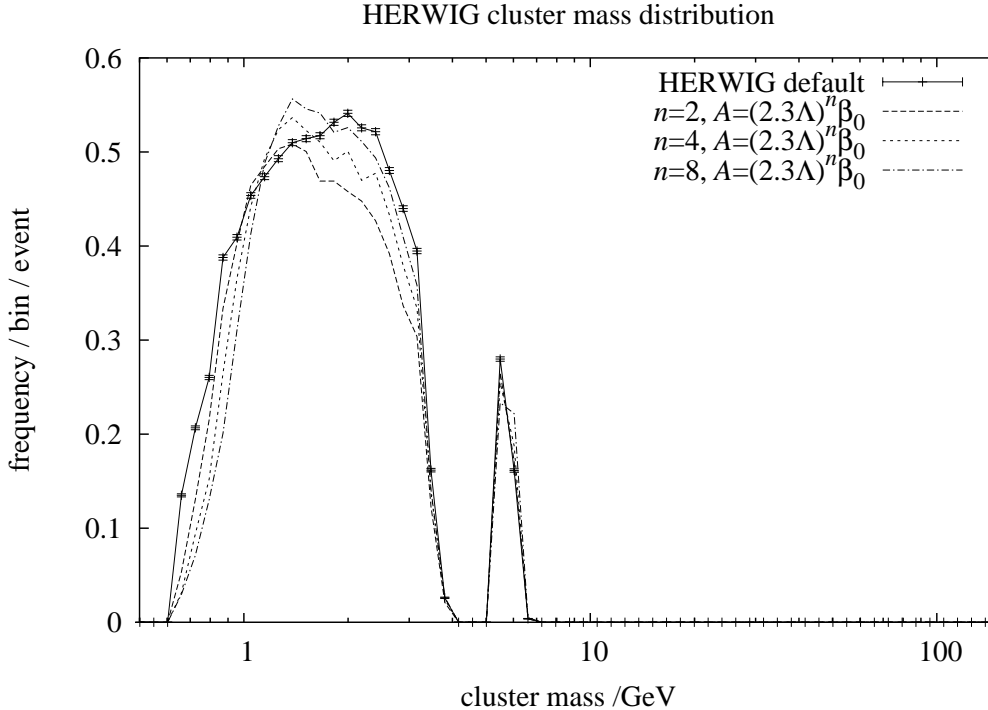


Figure 19: The cluster mass distribution generated using the α_S derived from power corrected beta function.

$(0.75 \text{ GeV})^2$. In HERWIG, the emission cut-off is implemented as being controlled by the gluon effective mass rather than as having a sharp cut-off, so that there is inevitably such a contribution. The proper study of this, taking account of the mass effects, is beyond our intention, and is presumably best left to a study incorporating experimental data, if possible using a generator that is based from the outset on the modified- α_S prescription rather than a modification of HERWIG as presented here.

One way to study the $g \rightarrow q\bar{q}$ dynamics might be to measure the compensation of the SU(2) light flavour charge. This should occur close to the electric charge compensation.

Let us now turn to a discussion of the analyticity of low energy α_S .

As stated above, the α_S defined by eqn. (6.5) has complex poles. This is unwelcome in the sense that it forbids a spectral representation, viz:

$$\alpha_S(Q^2) = - \int_0^\infty \frac{d\mu^2}{\mu^2 + Q^2} \rho_S(\mu^2), \quad (6.8)$$

where $\rho_S(\mu^2)$ is the spectral density function. As α_S is related to the gluon two-point function, the physical interpretation would be that in the confined vacuum the spectral density associated with the colour-octet state is ill-defined. On the other hand, colour-singlet two-point functions should have a valid spectral representation such that the complex poles must somehow cancel. We add that in our convention, a physical spectral density function is negative definite. However, if we impose this condition, we see that α_S must continue to grow towards low Q^2 .

We may rephrase this statement as follows. If colour is confined in the large distance limit, an α_S that describes the interaction of the unconfined gluon must vanish in the soft limit. But this is in violation of the spectral representation if the spectral density function is negative definite, such that there must be complex poles. These complex poles must cancel in quantities that are associated with colour singlet states.

Let us denote the above α_S , eqn. (6.5), that describes gluons both in the confined and the asymptotically-free vacuum, by $\alpha_S^{\text{glu.}}$. We then write the nonperturbative physics that cancels the poles by $\alpha_S^{\text{had.}}$. Then for the overall process of hadronization, we have:

$$\alpha_S^{\text{h}} = \alpha_S^{\text{glu.}} + \alpha_S^{\text{had.}}. \quad (6.9)$$

The former term is universal, but the latter term is not necessarily so. We also note that from the condition of finite emission probability, we required the first term to vanish as a power towards low Q^2 . This is natural considering that an unconfined gluon can not propagate in the confined vacuum. On the other hand, as the concept of emission probability does not hold much meaning in the hadronic phase, there is no such requirement governing the latter term except that it is confined to the region of small Q^2 , and it would be reasonable for it to remain non-zero.

Now let us shift contributions between the two terms such that there is no complex pole in either of the α_S , but the two terms, or more strictly their moments, are affected minimally, in some sense which we shall discuss later, for positive and real Q^2 . Then we can write:

$$\alpha_S^{\text{h}} = \alpha_S^{\text{conf.}} + \alpha_S^{\text{decay}}. \quad (6.10)$$

The former ‘confinement’ term is still at least almost universal. α_S^{decay} is expected to be the contribution to the observable under attention from the decay of the nonperturbative clusters and hadrons, and is expected to be effective at a lower scale than the former term.

scheme	$F_{1,1}$	$F_{2,1}$	$F_{3,1}$
$n = 2$	0.378	0.394	0.381
$n = 4$	0.394	0.419	0.401
$n = 6$	0.390	0.421	0.404
$n = 8$	0.385	0.420	0.404
Webber’s α_S	0.511	0.450	0.410

Table 1: First three moments, $F_{p,1}(2 \text{ GeV})$, of low energy α_S .

Using α_S^{h} which has a dispersive representation, as do its two constituents $\alpha_S^{\text{conf.}}$ and α_S^{decay} , we can calculate power corrections following the procedure of ref. [18]. When doing so, the quantities of main interest are the first few moments of α_S , i.e., $F_{p,1}(Q)$, where $F_{p,q}(Q)$ [15] are defined by:

$$F_{p,q}(Q) = \frac{p}{Q^p} \int_0^Q \frac{dk}{k} k^p [\alpha_S(k^2)]^q. \quad (6.11)$$

$\alpha_S^{\text{glu.}}$ has complex poles and therefore can not be used to calculate power corrections directly in the dispersive approach. However, if our argument above is correct, we can choose $\alpha_S^{\text{conf.}} \sim \alpha_S^{\text{glu.}}$. As these moments can be calculated numerically for any choice of α_S so long as it is integrable, it then follows that one may calculate them for $\alpha_S^{\text{glu.}}$ as an estimate of the moments of $\alpha_S^{\text{conf.}}$. We take the $n = 2, 4, 6$ and 8 cases with A set to $(2.3\Lambda)^n \beta_0$ and compare the result with α_S of ref. [15]. For $Q = 2$, the result is shown in tab. 1.

The α_S of ref. [15] is defined to describe event shapes and is therefore an α_S^h . Physically we would expect that both $\alpha_S^{\text{conf.}}$ and α_S^{decay} would be positive definite. If so, we have $\alpha_S^h > \alpha_S^{\text{conf.}}$. A more important criterion is that this is satisfied in the moments. We see from tab. 1 that this is indeed the case. Furthermore, we see that α_S^{decay} contribution only accounts for $\mathcal{O}(20\%)$ of the contribution to the moments.

From the requirement that α_S^{decay} mainly affects the region of Q^2 lower than $\alpha_S^{\text{conf.}}$, or more strictly $\alpha_S^{\text{glu.}}$, we expect that the higher moments of α_S^h and $\alpha_S^{\text{conf.}}$ are similar. This is also satisfied in tab. 1. However, the similarity is exaggerated by the choice of the cut-off scale, 2 GeV, which is high compared with the hadronic scale.

This argument governing the moments also implies that the moments $F_{p,1}(Q)$ derived from experimental data must be greater than the contribution from $\alpha_S^{\text{conf.}}$, such as those listed in tab. 1 except the one in the bottom row. From the data compiled in ref. [20], which we reproduce in tab. 2, $F_{1,1}(2 \text{ GeV})$ is in the range 0.391 to 0.560. Although 0.391 measured in the jet broadening observable B_W is quite low, it is not in contradiction of this statement.

Let us proceed to estimating the ambiguity of $F_{1,1}$ in the process of analytization in between eqns. (6.9) and (6.10). We can do this by simply subtracting off the complex poles in $\alpha_S^{\text{glu.}}$ and calculating the corresponding contribution to $F_{1,1}$. This analytization procedure is equivalent to that adopted in ref. [21].

We first define for u and v real:

$$u + iv = \frac{A}{\beta_0 Q^n}. \quad (6.12)$$

Then Q^2/Λ^2 is given by one of the roots:

$$\frac{Q^2}{\Lambda^2} = \left(\frac{A/(\beta_0 \Lambda^n)}{u + iv} \right)^{2/n} \equiv \left(\frac{a}{u + iv} \right)^{1/\nu}, \quad (6.13)$$

where we defined for convenience $a = A/(\beta_0 \Lambda^n)$ and $\nu = n/2$. Let us specialize in the case of even n . It turns out that out of the ν roots of eqn. (6.13), the only relevant one is the one whose phase is $1/\nu$ times the phase of $u - iv$, where this phase is taken to be between $-\pi$ and $+\pi$.

At the pole we have:

$$\alpha_S^{-1} = \beta_0 \log \left(\frac{Q^2}{\Lambda^2} \right) + \frac{2A}{nQ^n} = \beta_0 \left[\log \left(\frac{a}{u + iv} \right)^{1/\nu} + \frac{u + iv}{\nu} \right] = 0. \quad (6.14)$$

Hence:

$$u + iv = a \exp(u + iv), \quad (6.15)$$

from which we derive:

$$u = \frac{v}{\tan v}, \quad a = \frac{v}{e^u \sin v}. \quad (6.16)$$

Variable	$F_{1,1}(2 \text{ GeV})$
B_T	0.4508 ± 0.0225
B_W	0.3911 ± 0.0305
$1 - T$	0.4976 ± 0.0087
C	0.4527 ± 0.0110
M_h^2/Q^2	0.5602 ± 0.0224

Table 2: Moment $F_{1,1}(2 \text{ GeV})$ of low energy α_S , obtained by fit to event shape variables. Numbers taken from ref. [20].

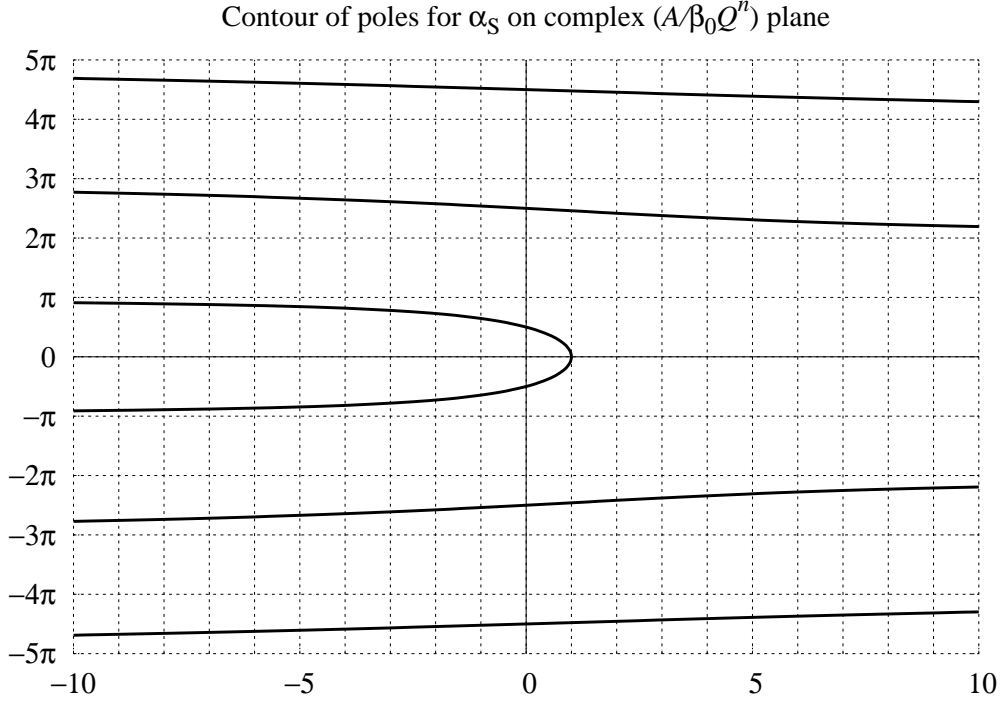


Figure 20: The contour of poles for α_S^{glu} on the complex $A/(\beta_0 Q^n)$ plane.

As a is positive, we require that $v/\sin v$ is also positive. With this condition, the contour of poles in the $u + iv$ space is plotted in fig. 20. a tends to $+0$ as $u \rightarrow +\infty$ and $+\infty$ as $u \rightarrow -\infty$.

Eqns. (6.16) are consistent with eqn. (6.14) only if:

$$|v| < \nu\pi. \quad (6.17)$$

Thus for $n = 2, 4$, there are two solutions which are complex conjugates, whereas for $n = 6, 8$ there are four solutions, and so on. We note furthermore that the lowest solution is complex only if $a > e^{-1}$.

The poles of α_S can be found for given A and hence a by solving eqns. (6.16) to obtain v and u in terms of a . The residue on the Q^2 plane is given in terms of the beta function evaluated at the pole, $\beta = \beta_0(1 - u - iv)$, as:

$$\text{residue} = \frac{Q^2}{\beta(Q^2)} \Big|_{Q^2 \text{ at pole}}. \quad (6.18)$$

When there is no complex pole, the spectral representation of eqn. (6.8) has the well-known solution in terms of the discontinuity of α_S on the negative real axis:

$$\rho_S(\mu^2) = \frac{1}{2\pi i} [\alpha_S(\mu^2 e^{i\pi}) - \alpha_S(\mu^2 e^{-i\pi})]. \quad (6.19)$$

As stated earlier, a physical ρ_S is negative definite in our convention. The generalization of eqns. (6.8) and (6.19) to include contribution from the complex poles yields:

$$\alpha_S(Q^2) = - \int_0^\infty \frac{d\mu^2}{\mu^2 + Q^2} \rho_S(\mu^2) - \sum_{\text{pole}} \left[\frac{1}{\beta(\mu^2)(1 - Q^2/\mu^2)} \right] \Bigg|_{\mu^2 \text{ at pole}}, \quad (6.20)$$

This general expression does not depend on the particular form of α_S but assumes that the complex singularities are all simple poles. α_S can be analytized by subtracting the complex poles, or by adding:

$$\delta\alpha_S(Q^2) = \sum_{\text{pole}} \left[\frac{1}{\beta(\mu^2)(1 - Q^2/\mu^2)} \right] \Bigg|_{\mu^2 \text{ at pole}}. \quad (6.21)$$

Applying the formulae to the α_S in eqn. (6.5), the resultant analytized α_S has a negative definite spectral density, given by:

$$\rho_S(\mu^2) = -\frac{1}{\beta_0} \left[\left[\log\left(\frac{\mu^2}{\Lambda^2}\right) + \frac{2A}{n\beta_0\mu^n} \right]^2 + \pi^2 \right]^{-1}. \quad (6.22)$$

n is assumed to be even. Denoting the analytized α_S by $\overline{\alpha_S}$, as $\overline{\alpha_S}$ continues to grow with decreasing Q^2 , $\overline{\alpha_S}(0)$ is a finite number, which can be calculated either by integrating eqn. (6.22), or more simply by summing eqn. (6.21) at $Q^2 = 0$, i.e., summing $1/\beta$ over the poles.

$\overline{\alpha_S}(Q^2)$ has an unphysical $1/Q^2$ behaviour at large Q^2 , which must be cancelled by additional contribution from ρ_S . This additional contribution can be defined as a negative definite quantity only if the sum of the residues Q^2/β , eqn. (6.18), is positive. By evaluating eqn. (6.18) in the $A \rightarrow \infty$ limit, we see that this is always satisfied when $\nu = n/2$ is even, but violated for odd ν when A is large.

The ambiguity of $F_{1,1}$ is estimated by integrating eqn. (6.21) according to eqn. (6.11). We obtain $\delta F_{1,1} = 0.071, 0.016$ and -0.052 respectively for $n = 2, 4$ and 8 . A , as before, is given by $(2.3\Lambda)^n \beta_0$.

We see that the ambiguity, amounting to up to $\sim 10\%$ of $F_{1,1}$, is under control. Had we started from the unmodified perturbative α_S [21], the corresponding $\delta F_{1,1}$ would be undefinable.

As the procedure followed here gives an estimate only, it is not possible to draw definitive conclusions based on these numbers, but comparison with tabs. 1 and 2 shows that the magnitude of $\delta F_{1,1}$ is consistent with data, and in our opinion $F_{1,1} + \delta F_{1,1}$, corresponding to $\overline{\alpha_S}$, also does not show disparity with tab. 2 that renders any particular choice of n completely unrealistic.

We have so far calculated the confinement contribution of eqn. (6.10) to $F_{1,1}$ and the ambiguity due to analytization in between eqns. (6.9) and (6.10). It is not possible to calculate the decay contribution within our present framework. A very naive expectation would be that since the decay process occurs at lower energies than the confinement process, the highest energy component of $\alpha_S^{\text{had.}}$ would be given by the same $\delta\alpha_S$ that cancels the

complex pole in α_S^{glu} . If we accept this, we would expect that although α_S^{had} is non-universal, its size is estimated by $\delta F_{1,1}$ that we have calculated above. Again, all cases are consistent with data and is in agreement with the small size of the α_S^{had} contribution to $F_{1,1}$ seen in tab. 1, or in the difference between tabs. 1 and 2.

One may ask how our results depend on the input parameters. We recall that we determined our value of A by tuning the peak position of α_S , as in eqn. (6.7). We may shift the peak position slightly and see how this affects our prediction. For $n = 4$, when Q_{peak} is modified from 0.575 GeV corresponding to $Q_{\text{min}} = 0.4$ GeV to 0.5 GeV corresponding to $Q_{\text{min}} = 0.25$ GeV, which we consider to be unreasonably small, $\delta F_{1,1}$ decreases from 0.015 to -0.004 , while $F_{1,1}$ from integrating α_S^{glu} itself increases from 0.394 to 0.424. We have also calculated the case $Q_{\text{peak}} = 0.65$ GeV such that $Q_{\text{min}} = 0.55$ GeV which again is unreasonable. This yields $\delta F_{1,1} = 0.032$ whereas $F_{1,1}$ is reduced to 0.369. We observe that $F_{1,1} + \delta F_{1,1}$ is less sensitive to A than $F_{1,1}$ itself is, and in any case the dependence is small enough to trust the numbers calculated using the procedures presented here.

7. Conclusions

We have reconsidered the phenomenon of local charge compensation from the viewpoint of colour-preconfined models of hadronization.

We have suggested that the study of minijet charge as a function of the resolution parameter $y_{\text{cut}} \propto k_{T\text{cut}}^2$ could provide information on the nature of dynamics governing hadronization. In particular, the scale at which local charge compensation is maximally violated, i.e., where the minijet charge is peaked, is the scale at which nonperturbative, confinement, dynamics sets in. We have demonstrated by simulations using HERWIG that modifications in the parameters governing hadronization could lead to significant differences in the behaviour of the minijet charge. We have made a comparison with PYTHIA and found that the predictions of the two generators are similar.

The values for minijet charge depend on the scheme used for clustering minijets. Our default procedure uses the Cambridge algorithm, but we have demonstrated that the combination of the JADE algorithm in the confined region and angular-ordered Durham algorithm in the perturbative region results in less contamination from misidentified tracks. We have proposed a ‘preclustered’ scheme which shows marked improvement compared with the other algorithms when the preclustering scale y_{had} is tuned to $(0.5 \text{ GeV})^2$.

In addition to the e^+e^- case, we have presented a simple analysis of the minijet charge at hadron collisions and found that due to the extra contamination in this case, the peak in the minijet charge is weakened. The peak disappears completely when the soft underlying events are added according to the default option of HERWIG.

We have studied a modification of the HERWIG default procedure to express the cluster-splitting dynamics at the end of the parton shower phase in terms of emissions that are considered unresolved in the course of the ordinary parton shower. Through this analysis, we have found that the lowest scale of cluster-splitting dynamics is about 0.4 GeV.

This analysis also suggests that because the product of neighbouring cluster masses is smaller in this case compared with the HERWIG default procedure, the peak height in the minijet charge is necessarily smaller than is suggested by HERWIG. On the other hand, the relaxation of HERWIG's sudden transition to the confinement phase is expected to smear this peak.

Our simulations for this part of the study were carried out using a simple modification of HERWIG with several approximations. It is hoped that simulation using Monte-Carlo event generators of the next generation, that are based from the outset on the modified- α_S prescription, will also be available in the future. We emphasize that comparison with experiment can nevertheless be made using our present approach to yield useful information that has less theoretical prejudice, but once a particular model of α_S is available, such as the one proposed in this paper, simulation based from the outset on modified- α_S could leave less ambiguity in the theoretical interpretation.

We have discussed the possible implications of our findings to the underlying nonperturbative dynamics. In particular, we studied a model in which the transition between the perturbative phase and the nonperturbative phase during the course of hadronization is driven by the semi-perturbative splitting $g \rightarrow q\bar{q}$, possibly enhanced by the string-like confining force. This gives rise to an α_S which vanishes as a power towards low Q^2 but has complex poles. We have argued, in agreement with available data, that the moments of this α_S gives an estimate of the part of the power corrections to event shapes that is universal and comes from soft gluon emission, whereas its complex poles give an estimate of the ambiguity, which is found to be small. In this picture, the remaining part of power corrections is related to the cascade decay of the nonperturbative, confined, clusters, and in our present framework can only be estimated to be of the same order as the ambiguity of the former part.

Acknowledgments

The author thanks Bryan Webber for inspiring and extensive discussions.

References

- [1] G. Marchesini, B. R. Webber, G. Abbiendi, I. G. Knowles, M. H. Seymour and L. Stanco, *HERWIG: A Monte Carlo event generator for simulating Hadron Emission Reactions With Interfering Gluons. Version 5.1 - April 1991*, *Comput. Phys. Commun.* **67** (1992) 465; G. Corcella, I.G. Knowles, G. Marchesini, S. Moretti, K. Odagiri, P. Richardson, M.H. Seymour and B.R. Webber, *HERWIG 6: An event generator for Hadron Emission Reactions With Interfering Gluons (including supersymmetric processes)*, *J. High Energy Phys.* **0101** (2001) 010 [[hep-ph/0011363](#)]; *HERWIG 6.5 release note*, [hep-ph/0210213](#).
- [2] T. Sjostrand, P. Eden, C. Friberg, L. Lonnblad, G. Miu, S. Mrenna and E. Norrbin, *High-energy-physics event generation with PYTHIA 6.1*, *Comput. Phys. Commun.* **135** (2001) 238 [[hep-ph/0010017](#)].
- [3] See, for example:

- A. V. Manohar and M. B. Wise, *Power suppressed corrections to hadronic event shapes*, *Phys. Lett.* **B 344** (1995) 407 [[hep-ph/9406392](#)];
- B. R. Webber, *Estimation of power corrections to hadronic event shapes*, *Phys. Lett.* **B 339** (1994) 148 [[hep-ph/9408222](#)];
- Y. L. Dokshitzer and B. R. Webber, *Calculation of power corrections to hadronic event shapes*, *Phys. Lett.* **B 352** (1995) 451 [[hep-ph/9504219](#)];
- Y. L. Dokshitzer and B. R. Webber, *Power corrections to event shape distributions*, *Phys. Lett.* **B 404** (1997) 321 [[hep-ph/9704298](#)];
- Y. L. Dokshitzer, A. Lucenti, G. Marchesini and G. P. Salam, *On the universality of the Milan factor for $1/Q$ power corrections to jet shapes*, *J. High Energy Phys.* **9805** (1998) 003 [[hep-ph/9802381](#)];
- G. P. Korchemsky and S. Tafat, *On power corrections to the event shape distributions in QCD*, *J. High Energy Phys.* **0010** (2000) 010 [[hep-ph/0007005](#)];
- E. Gardi and J. Rathsmann, *Renormalon resummation and exponentiation of soft and collinear gluon radiation in the thrust distribution*, *Nucl. Phys.* **B 609** (2001) 123 [[hep-ph/0103217](#)].
- [4] D. Amati and G. Veneziano, *Preconfinement As A Property Of Perturbative QCD*, *Phys. Lett.* **B 83** (1979) 87.
- [5] Y. L. Dokshitzer and S. I. Troian, *Nonleading Perturbative Corrections To The Dynamics Of Quark - Gluon Cascades And Soft Hadron Spectra In $E^+ E^-$ Annihilation*, LENINGRAD-84-922;
Y. I. Azimov, Y. L. Dokshitzer, V. A. Khoze and S. I. Troian, *The String Effect And QCD Coherence*, *Phys. Lett.* **B 165** (1985) 147; *Similarity Of Parton And Hadron Spectra In QCD Jets*, *Z. Physik* **C 27** (1985) 65.
- [6] H. Akimoto, A. Beretvas and S. Geer, *CDF note 4083* (1997).
- [7] A. Krzywicki and B. Petersson, *Breakdown Of Hadronic Scaling Or Evidence For Clustering?*, *Phys. Rev.* **D 6** (1973) 924;
C. Bromberg *et al.*, *The Charge Structure Of Multiparticle Final States In $P P$ Collisions At 102-GeV/C And 400-GeV/C*, *Phys. Rev.* **D 12** (1975) 1224.
- [8] B. R. Webber, *A QCD Model For Jet Fragmentation Including Soft Gluon Interference*, *Nucl. Phys.* **B 238** (1984) 492.
- [9] Yu.L. Dokshitzer, contribution cited in Report of the Hard QCD Working Group, Proc. Workshop on Jet Studies at LEP and HERA, Durham, December 1990, *J. Phys.* **G 17** (1991) 1537.
- [10] Y. L. Dokshitzer, G. D. Leder, S. Moretti and B. R. Webber, *Better jet clustering algorithms*, *J. High Energy Phys.* **9708** (1997) 001 [[hep-ph/9707323](#)].
We thank Bryan Webber for making available to us the FORTRAN code for various jet clustering algorithms.
- [11] W. Bartel *et al.* [JADE Collaboration], *Experimental Evidence For Differences In $P(T)$ Between Quark Jets And Gluon Jets*, *Phys. Lett.* **B 123** (1983) 460; *Experimental Studies On Multi - Jet Production In $E^+ E^-$ Annihilation At Petra Energies*, *Z. Physik* **C 33** (1986) 23.
- [12] R. Barate *et al.* [ALEPH Collaboration], *Determination of A_{FB}^b using jet charge measurements in Z decays*, *Phys. Lett.* **B 426** (1998) 217.

- [13] S. Catani, Y. L. Dokshitzer, M. H. Seymour and B. R. Webber, *Longitudinally invariant k_{\perp} -clustering algorithms for hadron-hadron collisions*, *Nucl. Phys.* **B 406** (1993) 187.
- [14] J. M. Butterworth, J. R. Forshaw and M. H. Seymour, *Multiparton interactions in photoproduction at HERA*, *Z. Physik* **C 72** (1996) 637 [[hep-ph/9601371](#)];
I. Borozan and M. H. Seymour, *An eikonal model for multiparticle production in hadron hadron interactions*, *J. High Energy Phys.* **0209** (2002) 015 [[hep-ph/0207283](#)].
- [15] B. R. Webber, *QCD power corrections from a simple model for the running coupling*, *J. High Energy Phys.* **9810** (1998) 012 [[hep-ph/9805484](#)].
- [16] G. Marchesini and B. R. Webber, *Simulation Of QCD Jets Including Soft Gluon Interference*, *Nucl. Phys.* **B 238** (1984) 1.
Our notation follows:
R. K. Ellis, W. J. Stirling and B. R. Webber, ‘*QCD and Collider Physics*’, Cambridge University Press (1996).
- [17] G. Gustafson and U. Pettersson, *Dipole Formulation Of QCD Cascades*, *Nucl. Phys.* **B 306** (1988) 746;
L. Lonnblad, *ARIADNE version 4: A Program for simulation of QCD cascades implementing the color dipole model*, *Comput. Phys. Commun.* **71** (1992) 15.
- [18] Y. L. Dokshitzer, G. Marchesini and B. R. Webber, *Dispersive Approach to Power-Behaved Contributions in QCD Hard Processes*, *Nucl. Phys.* **B 469** (1996) 93 [[hep-ph/9512336](#)].
- [19] For a recent lattice simulation, see: S. Aoki *et al.* [JLQCD Collaboration], *Light hadron spectroscopy with two flavors of $O(a)$ -improved dynamical quarks*, [hep-lat/0212039](#).
- [20] Y. L. Dokshitzer, G. Marchesini and G. P. Salam, *Revisiting non-perturbative effects in the jet broadenings*, *Eur. Phys. J. Direct.* **C 1** (1999) 3 [[hep-ph/9812487](#)].
- [21] D. V. Shirkov and I. L. Solovtsov, *Analytic QCD running coupling with finite IR behaviour and universal $\bar{\alpha}_S(0)$ value*, *JINR Rapid Comm.* **No. 2 [76]** (1996) 5 [[hep-ph/9604363](#)];
Analytic model for the QCD running coupling with universal $\bar{\alpha}_S(0)$ value, *Phys. Rev. Lett.* **79** (1997) 1209 [[hep-ph/9704333](#)];
D. V. Shirkov, *On the analytic *causal* model for the QCD running coupling*, *Nucl. Phys.* **64 (Proc. Suppl.)** (1998) 106 [[hep-ph/9708480](#)].